Eight derivatives bearing 5-nitro-furan phenyl ester core were examined as shown in Table 2. A similar degree of inhibitory activity was observed for the analogs having a hydroxy group at the *meta* or *para* position of phenyl ring (**9**–**11**). While substitution of the hydroxy group with acetyl group showed a similar degree of inhibitory activity (**12**), substitution with ethyl-ester increased compound potency (**13**). Further, introduction of methoxy group at the *ortho* position also increased compound potency (**14**). The compound containing methoxy-carbonyl and methoxy groups at the *para* or *ortho* positions exhibited a fine inhibitory activity (**15**). Introduction of phenyl-methyl-amine at the *para* position also maintained compound potency (**16**).

Eleven derivatives bearing 5-nitro-furan ester core bound with benzyl-based substitutes were investigated as summarized in Table 3. Connection of a benzyl group without any additional functional substitute showed moderate inhibitory activity (**17**). Attaching nitro group, methoxy-ether, or *tert*-butoxy-ester exhibited slight changes in compound potency (**18**–**20**). Extension of alkyl chain caused no significant difference in inhibitory potency (**21**). However, addition of hydroxy group decreased inhibitory activity (**22**). Introduction of methoxy group further decreased compound potency regardless of the position of the group bound to phenyl ring (**23**–**25**). While connection of two methoxy groups improved compound potency (**26**), replacement of two methoxy groups by chlorides showed low inhibitory activity (**27**).

Six derivatives were synthesized by changing the ester bond with carbonyl group as shown in Table 4. Ester linkage is disadvantageous for medicine because esterase digests the linkage and the drug concentration in a body decreases rapidly. Nitro-phenyl group was connected to the carbonyl carbon with changing the length of alkyl chain and the position of nitro group (**28**–**30**). None of the derivatives showed noticeable inhibitory activity. The ester linkage was replaced by an amide bond (**31**–**33**), in which hydroxy-methyl-benzyl, acetyl-methyl-benzyl, or bromo-methyl-benzyl was bound *via* a carbamoyl group. This modification also resulted in complete loss of compound potency.

Table 2. RNase H Inhibitory Activity and Cytotoxicity of the Derivatives Bearing Phenyl Ester Core

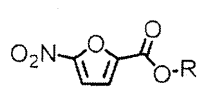

Compound	–O–R	IC_{50} (μM)	CC_{50} (μM)
9	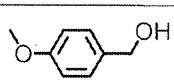	7.2	>100
10	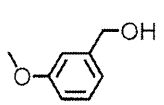	8.2	24
11	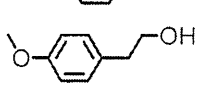	9.1	>100
12	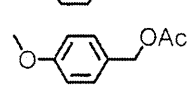	8.7	49
13	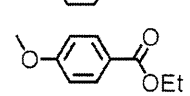	3.6	>100
14	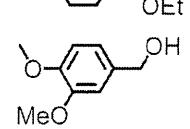	3.1	>100
15	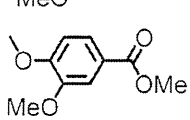	1.4	>100
16	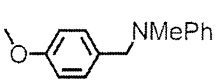	3.8	>100

Cytotoxicity was little or undetectable for most of the derivatives modulated at the nitro-furan moiety except for compound **5** (Table 1). No detectable cytotoxicity was also observed for most of the derivatives bearing nitro-furan-phenyl ester core (Table 2). It should be noted that highly active compounds, **14** and **15**, showed no noticeable cytotoxicity at a concentration of 100 μM. In contrast, the analogs bearing ester core bound with benzyl-based substitute showed some degree of cytotoxicity (Table 3). Further, the analogs converted the ester into amide or ketone showed cytotoxicity in which CC_{50} ranged from 9 to 32 μM (Table 4). Overall, in the measurement using 293T cells, half of the synthesized compounds showed noticeable cytotoxicity but almost all of the toxicity-detected compounds showed little RNase H inhibitory activity. Accordingly, the results of this assay suggest that active compounds have no significant cytotoxicity and the nitro-furan-phenyl ester skeleton is the most favorable among them from a cytotoxic viewpoint.

In order to examine the stability of the binding structure of a potent compound inside the active site of the target protein, MD simulation was performed for the complex of a synthesized derivative **15** and RNase H domain. MD simulation was carried out for 20 ns and root mean square deviation (RMSD) relative to the structure after heating was calculated as shown in Fig. S1 of the supplemental information. The RMSD value showed a gradual increase up to 5 ns and scarcely changed during later 15 ns. Accordingly, the binding conformation of the complex was judged to be equilibrated. In order to extract the snapshot structure representing a typical binding mode of compound **15** and RNase H domain, the averaged structure was obtained using 2500 trajectories from the last 5 ns of MD simulation. The RMSD between each trajectory and the average structure was calculated, and then one trajectory with the smallest RMSD value was determined to be the typical complex structure shown in Fig. 1a.

Two Mg^{2+} ions were held by the side chains of four acid residues; Asp443, Glu478, Asp498, Asp549, and the compound was stably bound to the active site without changing the binding mode during 20 ns simulation. In the binding structure, the nitro-furan-ester core is especially, stably bound to two Mg^{2+} ions as shown in Fig. 1a. A stereo view of the binding structure is presented in Fig. S2 of the supplemental information. The oxygen atom on the furan ring is oriented toward the divalent metals. Nitro oxygen and carbonyl oxygen of the ester are strongly coordinated to the respective Mg^{2+} ions. Therefore, a large ring-shaped configuration of –Mg–O–N–C–O–C–C–O–Mg– is formed. The inter-atomic distance between two Mg^{2+} ions is 3.8 Å. The distance between the nitro oxygen atom and one Mg^{2+} ion is 1.9 Å, and that between carbonyl oxygen and the other Mg^{2+} ion is also 1.9 Å. Figure

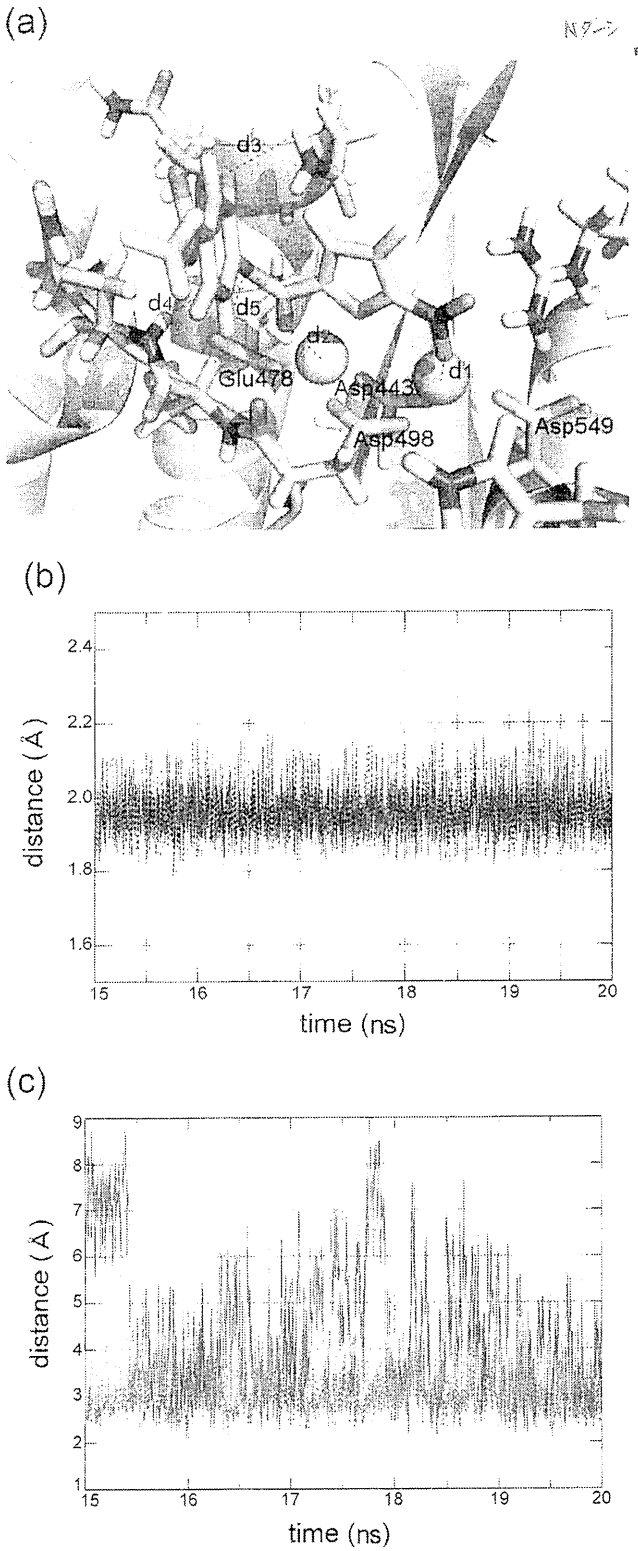

Fig. 1. (a) Binding Structure of an Active Compound to the RNase H Domain, Obtained by MD Simulation

Compound and several polar residues are shown in stick representation. Two Mg^{2+} ions are denoted by spheres. (b) Changes in the distances between nitro oxygen and Mg^{2+} ion (d_1: red solid line) and between carbonyl oxygen and another Mg^{2+} ion (d_2: blue dotted line) for the last 5 ns of MD simulation. (c) Changes in the distances between methoxy oxygen and amino hydrogen of Asn474 (d_3: green solid line), between ester oxygen and amide hydrogen of main chain of Gln500 (d_4: cyan broken line), and between ester oxygen and Cα hydrogen of Ser499 (d_5: yellow dotted line) for the last 5 ns of MD simulation.

1b shows the changes of these two distances for the last 5 ns of MD simulation. These graphs clearly indicate that the interaction of oxygen atom and Mg^{2+} ion is quite strong and that the oxygen-Mg interaction is essentially important for the binding of potent compound.

Methoxy-carbonyl and methoxy groups connected to phenyl stick out from the binding pocket. The distance between methoxy oxygen and hydrogen atom of amino group of Asn474 was monitored as shown in Fig. 1c. The distance largely fluctuates during the simulation and the interaction is not so steady. Hence, there is much room for improvement in this region. The oxygen atom at the ester bond has noticeable interactions with the amide group of main chain of Gln500. The change of the distance between the ester oxygen and the hydrogen atom of the amide group is shown in Fig. 1c. No abrupt, large change is observed in the distance. Therefore, the interaction contributes to stabilizing the binding of the potent compound. The distance between the ester oxygen and the Cα hydrogen atom of Ser 499 was also monitored. The distance shows no large change for the last 5 ns of simulation, which suggests the stability of the binding of the ester part with RNase H domain. Consequently, it is confirmed from the MD simulation that an active compound **15** is stably bound to the active site of the RNase H domain with coordinating to two divalent metal ions and making supportive interaction at the ester part.

Discussion

According to the data summarized in Table 3, it is suggested that various kinds of functional groups connected to the benzyl ring have little interaction with the RNase H domain and that the functional group-binding region is located outside the binding pocket and is exposed to the solvent. Further, a comparison of inhibitory activity between compounds **17**–**20** and compounds **21**–**27** suggests that the length of alkyl chain connecting to phenyl ring has a significant influence on the difference in compound potency. That is, the longer alkyl chain in compounds **21**–**27** is less favorable in terms of both inhibitory activity and cytotoxicity. This indicates that a strategy to increase the inhibitory activity is to position the substitute closer to the nitro-furan group. The conversion may allow the aromatic ring or substitute to interact with the target protein inside the binding pocket.

A comparison of inhibitory activities of compounds in Tables 2 and 3 indicates that the introduction of phenyl-ester connected to nitro-furan shows higher compound potency than that of benzyl-ester. This is consistent with the findings described above paragraph and supports the notion that the compound potency increases when the position of the substitute connected to the ester linkage is closer to the nitro-furan. The incorporation of polarized substitutes like methoxy, hydroxy, methoxy-carbonyl, or ethoxy-carbonyl group is effective to increase the compound potency. In particular, the introduction of methoxy group at the *ortho*-position of phenyl ring effectively increases the inhibitory activity.

All the compounds in Tables 2 and 3 have the ester linkage. The data summarized in Table 4 clearly indicate that conversion of the ester linkage into carbonyl and/or amide bond results in loss of inhibitory potency. Both bonds will be likely to make the chemical to be in a straight configuration. If a compound has a straight form, the side part of the compound

Table 3. RNase H Inhibitory Activity and Cytotoxicity of the Derivatives Bearing Ester Core Bound with Benzyl-Based Substitute

Compound	–O–R	IC_{50} (μM)	CC_{50} (μM)
17	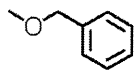	5.4	38
18	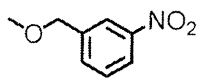	5.0	>100
19	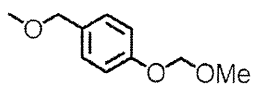	5.8	75
20	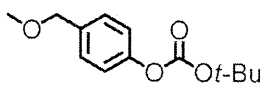	4.5	>100
21	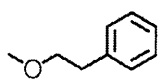	5.1	57
22	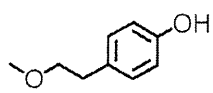	7.9	39
23	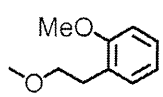	14.2	42
24	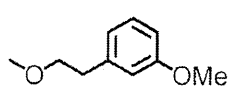	18.6	36
25	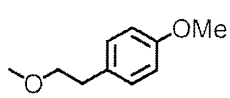	12.5	36
26	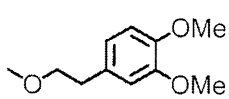	8.5	51
27	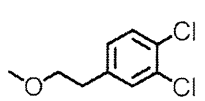	17.4	64

Table 4. RNase H Inhibitory Activity and Cytotoxicity of the Derivatives Converted the Ester Bond into Other Kinds of Linkages

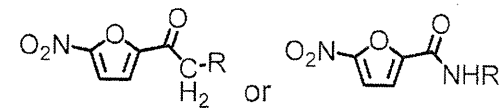

Compound	$-CH_2-R$ or –NH–R	IC_{50} (μM)	CC_{50} (μM)
28	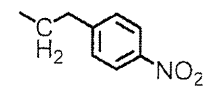	>50	11
29	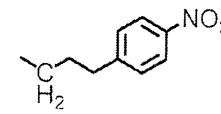	>50	17
30	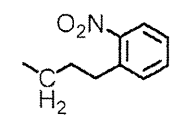	>50	9
31	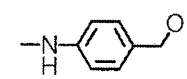	>50	29
32	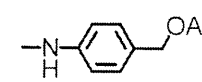	>50	27
33	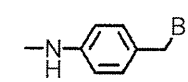	>50	32

will collide with the inside wall of the binding pocket of the RNase H domain. Accordingly, compounds are hardly combined with the binding pocket.

The conversion of the nitro-furan group into pyrrole drastically decreases the inhibitory activity while conversion to nitro-thiophen maintains the activity (Table 1). This indicates that a nitro-furan or nitro-thiophene core is indispensable for inhibitory potency. The characteristic property of nitro-furan is its large electric polarity. Oxygen atoms are negatively charged and these oxygen atoms will be coordinated to divalent metal ions at the RNase H active site. The attachment of non-polar substitute to furan results in decrease of compound potency. Accordingly, the 3rd and 4th positions of furan become close to the residues inside the RNase H active site.

RNase H of HIV-1 exerts its enzymatic activity by incorporating divalent metal ions at the reaction site.[38,39] It had been controversial how many metal ions were required at the RNase H reaction site to exert its enzymatic activity.[40] A theoretical study by De Vivo *et al.* suggested that the presence of two divalent metal ions is essential for RNase H activity and that two metal ions act cooperatively with facilitating the binding of a substrate and catalyzing the enzymatic reaction.[41] This theoretical finding strongly suggests double coordination of divalent metal ions at the RNase H domain. Crystal structures on the complex of the RNase H domain and its inhibitor were successively reported from three different research groups.[23,25–27] All of the crystal structures ever reported showed the presence of two metal ions at the active site. One of the divalent metal ions was held deep inside the binding pocket of the RT RNase H domain with making coordination bonds to three carboxyl groups of Asp443, Glu478 and Asp498. The other was fixed with making coordination bonds to two carboxyl groups of Asp443 and Asp549. The distance between two metal ions was about 4 Å. Every inhibitor in crystal structures was revealed to have a similar binding mode. That is, inhibitors are stabilized with forming coordination bonds to both metal ions. Accordingly, it is highly probable that the chemical compounds showing RNase H inhibitory activity examined in this study are also coordinated to two divalent metal ions. Hence, negatively charged oxygen atoms of the nitro group, furan, and carbonyl group are aligned in a straight form. This negatively charged region will be attached to the divalent metal ions.

The binding structure deduced from MD simulation indicates that ether oxygen at the ester bond has an interaction with a polar residue, Ser499, which is located at the deep inside of RNase H domain. This residue would have little influence on the function of RNase H. Therefore, one of the

designs to improve inhibitory activity is to modify the compound to bear some polar functional group that enables a strong interaction with Ser499. In order to enhance the binding affinity of the compounds with RNase H active site, the incorporation of a polar functional group bound to phenyl ring is one of the possible conversions of our derivatives. The distance between methoxy group and the amine of Asn474 largely fluctuated during MD simulation. If the interaction with Asn474 is enforced, compound will be more stably combined with the RNase H domain.

Conclusion

More than 30 chemical compounds were synthesized for developing the inhibitors of RNase H activity of HIV-1 reverse transcriptase. Inhibitory potency of RNase H enzymatic activity was measured in a biochemical assay with a real-time fluorescence monitoring method. The active compounds found in our previous studies commonly bear nitro-furan ring connecting to hydrophobic region *via* an ester linkage. Conversion of the nitro-furan group into pyrrole drastically decreased the inhibitory activity while conversion into nitro-thiophene maintained the compound potency. This means that the structural basis of nitro-furan or nitro-thiophene is indispensable for inhibitory activity. An improvement in compound potency was observed when a phenyl-ester moiety was connected to the nitro-furan and further methoxy-carbonyl and methoxy groups were bound to the phenyl ring. No notable change in inhibitory potency was observed when benzyl-ester based substitute was connected to nitro-furan. Modulation of ester linkage resulted in complete loss of compound potency. Molecular dynamics simulation was performed to examine the stability of the binding structure of a synthesized active compound to RNase H domain. It was demonstrated that a potent compound was stably bound to the active site with establishing strong coordinate bonds with divalent metal ions located at the active site. The present study provides important information for designing prospective chemical structures inhibiting HIV-1 RNase H activity.

Acknowledgments This work was supported by a Health and Labor Science Research Grant for Research on Publicly Essential Drugs and Medical Devices from the Ministry of Health and Labor of Japan. A part of this work was also supported by a Grant-in-Aid for Scientific Research (C) from Japan Society for the Promotion of Science (JSPS). Theoretical calculations were performed at the Research Center for Computational Science, Okazaki, Japan and at the Information Technology Center of the University of Tokyo and also by the high-performance computer system at Institute for Media Information Technology in Chiba University.

References

1) Goody R. S., Müller B., Restle T., *FEBS Lett.*, **291**, 1–5 (1991).
2) Ren J., Stammers D. K., *Virus Res.*, **134**, 157–170 (2008).
3) Andréola M. L., De Soultrait V. R., Fournier M., Parissi V., Desjobert C., Litvak S., *Expert Opin. Ther. Targets*, **6**, 433–446 (2002).
4) Klumpp K., Mirzadegan T., *Curr. Pharm. Des.*, **12**, 1909–1922 (2006).
5) Tramontano E., *Mini Rev. Med. Chem.*, **6**, 727–737 (2006).
6) Tanese N., Telesnitsky A., Goff S. P., *J. Virol.*, **65**, 4387–4397 (1991).
7) Telesnitsky A., Goff S. P., *EMBO J.*, **12**, 4433–4438 (1993).
8) Borkow G., Fletcher R. S., Barnard J., Arion D., Motakis D., Dmitrienko G. I., Parniak M. A., *Biochemistry*, **36**, 3179–3185 (1997).
9) Tramontano E., Esposito F., Badas R., Di Santo R., Costi R., La Colla P., *Antiviral Res.*, **65**, 117–124 (2005).
10) Tarrago-Litvak L., Andreola M. L., Fournier M., Nevinsky G. A., Parissi V., de Soultrait V. R., Litvak S., *Curr. Pharm. Des.*, **8**, 595–614 (2002).
11) Cowan J. A., Ohyama T., Howard K., Rausch J. W., Cowan S. M., Le Grice S. F., *J. Biol. Inorg. Chem.*, **5**, 67–74 (2000).
12) Haren L., Ton-Hoang B., Chandler M., *Annu. Rev. Microbiol.*, **53**, 245–281 (1999).
13) Steitz T. A., Smerdon S. J., Jäger J., Joyce C. M., *Science*, **266**, 2022–2025 (1994).
14) Nowtny M., Gaidamakov S. A., Crouch R. J., Yang W., *Cell*, **121**, 1005–1016 (2005).
15) Nowtny M., Gaidamakov S. A., Crouch R. J., Yang W., *EMBO J.*, **25**, 1924–1933 (2006).
16) Shaw-Reid C. A., Munshi V., Graham P., Wolfe A., Witmer M., Danzeisen R., Olsen D. B., Carrol S. S., Embrey M., Wai J. S., Miller M. D., Cole J. L., Hazuda D. J., *J. Biochem.*, **278**, 2777–2780 (2003).
17) Hang J. Q., Rajendran S., Yang Y., Li Y., In P. W. K., Overton H., Parkes K. E. B., Cammack N., Martin J. A., Klumpp K., *Biochem. Biophys. Res. Commun.*, **317**, 321–329 (2004).
18) Budihas S. R., Gorshkova I., Gaidamakov S., Wamiru A., Bona M. K., Parniak M. A., Crouch R. J., McMahon J. B., Beutler J. A., Le Grice S. F., *Nucleic Acids Res.*, **33**, 1249–1256 (2005).
19) Fuji H., Urano E., Futahashi Y., Hamatake M., Tatsumi J., Hoshino T., Morikawa Y., Yamamoto N., Komano J., *J. Med. Chem.*, **52**, 1380–1387 (2009).
20) Yanagita H., Urano E., Matsumoto K., Ichikawa R., Takaesu Y., Ogata M., Murakami T., Wu H. G., Chiba J., Komano J., Hoshino T., *Bioorg. Med. Chem.*, **19**, 816–825 (2011).
21) Chan K. C., Budihas S. R., Le Grice S. F., Parniak M. A., Crouch R. J., Gaidamakov S. A., Isaaq H. J., Wamiru A., McMahon J. B., Beutler J. A., *Anal. Biochem.*, **331**, 296–302 (2004).
22) Parniak M. A., Min K. L., Budihas S. R., Le Grice S. F., Beutler J. A., *Anal. Biochem.*, **322**, 33–39 (2003).
23) Lansdon E. B., Liu Q., Leavitt S. A., Balakrishnan M., Perry J. K., Lancaster-Moyer C., Kutty N., Liu X., Squires N. H., Watkins W. J., Kirschberg T. A., *Antimicrob. Agents Chemother.*, **55**, 2905–2915 (2011).
24) Martí-Renom M. A., Stuart A. C., Fiser A., Sánchez R., Melo F., Sali A., *Annu. Rev. Biophys. Biomol. Struct.*, **29**, 291–325 (2000).
25) Kirschberg T. A., Balakrishnan M., Squires N. H., Barnes T., Brendza K. M., Chen X., Eisenberg E. J., Jin W., Kutty N., Leavitt S., Liclican A., Liu Q., Liu X., Mak J., Perry J. K., Wang M., Watkins W. J., Lansdon E. B., *J. Med. Chem.*, **52**, 5781–5784 (2009).
26) Himmel D. M., Maegley K. A., Pauly T. A., Bauman J. D., Das K., Dharia C., Clark A. D. Jr., Ryan K., Hickey M. J., Love R. A., Hughes S. H., Bergqvist S., Arnold E., *Structure*, **17**, 1625–1635 (2009).
27) Su H. P., Yan Y., Prasad G. S., Smith R. F., Daniels C. L., Abeywickrema P. D., Reid J. C., Loughran H. M., Kornienko M., Sharma S., Grobler J. A., Xu B., Sardana V., Allison T. J., Williams P. D., Darke P. L., Hazuda D. J., Munshi S., *J. Virol.*, **84**, 7625–7633 (2010).
28) Li H., Robertson A. D., Jensen J. H., *Proteins*, **61**, 704–721 (2005).
29) Cieplak P., Cornell W. D., Bayly C., Kollman P. A., *J. Comput. Chem.*, **16**, 1357–1377 (1995).
30) Matsuyama S., Aydan A., Ode H., Hata M., Sugiura W., Hoshino T., *J. Phys. Chem. B*, **114**, 521–530 (2010).
31) Sano E., Li W., Yuki H., Liu X., Furihata T., Kobayashi K., Chiba K., Neya S., Hoshino T., *J. Comput. Chem.*, **31**, 2746–2758 (2010).
32) Ode H., Neya S., Hata M., Sugiura W., Hoshino T., *J. Am. Chem.*

Soc., **128**, 7887–7895 (2006).

33) Ode H., Matsuyama S., Hata M., Neya S., Kakizawa J., Sugiura W., Hoshino T., *J. Mol. Biol.*, **370**, 598–607 (2007).

34) Jorgensen W. L., Chandrasekhar J., Madura J. D., Impey R. W., Klein M. L., *J. Chem. Phys.*, **79**, 926–935 (1983).

35) Case D. A., Darden T. A., Cheatham T. E. III, Simmerling C. L., Wang J., Duke R. E., Luo R., Merz K. M., *et al.*, "AMBER 9," University of California, San Francisco, 2006.

36) Katagiri D., Fuji H., Neya S., Hoshino T., *J. Comput. Chem.*, **29**, 1930–1944 (2008).

37) Ryckaert J.-P., Ciccotti G., Berendsen H. J. C., *J. Comput. Phys.*, **23**, 327–341 (1977).

38) Sarafianos S. G., Das K., Tantillo C., Clark A. D. Jr., Ding J., Whitcomb J. M., Boyer P. L., Hughes S. H., Arnold E., *EMBO J.*, **20**, 1449–1461 (2001).

39) Huang H., Chopra R., Verdine G. L., Harrison S. C., *Science*, **282**, 1669–1675 (1998).

40) Klumpp K., Hang J. Q., Rajendran S., Yang Y., Derosier A., Wong Kai In P., Overton H., Parkes K. E., Cammack N., Martin J. A., *Nucleic Acids Res.*, **31**, 6852–6859 (2003).

41) De Vivo M., Dal Peraro M., Klein M. L., *J. Am. Chem. Soc.*, **130**, 10955–10962 (2008).

Journal of Cellular Physiology

Dys-Regulated Activation of a Src Tyroine Kinase Hck at the Golgi Disturbs *N*-Glycosylation of a Cytokine Receptor Fms

RANYA HASSAN,[1] SHINYA SUZU,[1] MASATERU HIYOSHI,[1] NAOKO TAKAHASHI-MAKISE,[1] TAKAMASA UENO,[2] TSUTOMU AGATSUMA,[3] HIROFUMI AKARI,[4] JUN KOMANO,[5] YUTAKA TAKEBE,[6] KAZUO MOTOYOSHI,[7] AND SEIJI OKADA[1]*

[1]*Division of Hematopoiesis, Center for AIDS Research, Kumamoto University, Kumamoto, Kumamoto, Japan*

[2]*Viral Immunology, Center for AIDS Research, Kumamoto University, Kumamoto, Kumamoto, Japan*

[3]*Tokyo Research Laboratories, Kyowa Hakko Co., Ltd, Machida, Tokyo, Japan*

[4]*Laboratory of Disease Control, Tsukuba Primate Research Center, National Institute of Biomedical Innovation, Tsukuba, Ibaraki, Japan*

[5]*Laboratory of Virology and Pathogenesis, AIDS Research Center, National Institute of Infectious Diseases, Shinjuku, Tokyo, Japan*

[6]*Laboratory of Molecular Biology and Epidemiology, AIDS Research Center, National Institute of Infectious Diseases, Shinjuku, Tokyo, Japan*

[7]*Department of Internal Medicine, National Defense Medical College, Tokorozawa, Saitama, Japan*

HIV-1 Nef accelerates the progression to AIDS by binding with and activating a Src kinase Hck, but underlying molecular basis is not understood. We revealed that Nef disturbed *N*-glycosylation/trafficking of a cytokine receptor Fms in an Hck-dependent manner, a possible trigger to worsen uncontrolled immune system. Here, we provide direct evidence that dys-regulated activation of Hck pre-localized to the Golgi apparatus causes this Fms maturation arrest. A striking change in Hck induced by Nef other than activation was its skewed localization to the Golgi due to predominant Golgi-localization of Nef. Studies with different Nef alleles and their mutants showed a clear correlation among higher Nef-Hck affinity, stronger Hck activation, severe Golgi-localization of Hck and severe Fms maturation arrest. Studies with a newly discovered Nef-Hck binding blocker 2c more clearly showed that skewed Golgi-localization of active Hck was indeed the cause of Fms maturation arrest. 2c blocked Nef-induced skewed Golgi-localization of an active form of Hck (Hck-P2A) and Fms maturation arrest by Nef/Hck-P2A, but showed no inhibition on Hck-P2A kinase activity. Our finding establishes an intriguing link between the pathogenesis of Nef and a newly emerging concept that the Golgi-localized Src kinases regulate the Golgi function.

J. Cell. Physiol. 221: 458–468, 2009.

Studies of HIV-1-infected patients and monkey models have demonstrated that Nef, a protein with no enzymatic activity encoded by the HIV-1 genome, is a critical determinant for the development of AIDS (Kestler et al., 1991; Deacon et al., 1995; Kirchhoff et al., 1995). Subsequent studies of HIV-1 transgenic (Tg) mice supported the idea. The expression of entire coding sequences of HIV-1 in $CD4^+$ T cells and macrophages caused an AIDS-like disease, which was abolished by Nef deletion (Hanna et al., 1998). This pathogenetic activity of Nef is supposed to be mediated by its binding with cellular proteins, and a well-defined partner of Nef is Hck (Saksela et al., 1995), a member of Src family tyrosine kinases expressed in macrophages. Other Src kinases (Lyn, Fyn, c-Src, and Lck) bind Nef but with lower affinities (Arold et al., 1998; Karkkainen et al., 2006; Trible et al., 2006). Importantly, the disruption of proline-rich PxxP motif of Nef, an essential motif to bind the Src homology 3 (SH3) domain of Hck, was sufficient to protect Tg mice from the AIDS-like disease, and wild-type Nef-induced disease progression was significantly delayed in $Hck^{-/-}$ mice (Hanna et al., 2001), indicating that high affinity Nef-Hck binding in macrophages is at least in part responsible for disease development and progression. However, unresolved issue is how Nef-Hck binding followed by activation of Hck (Moarefi et al., 1997; Lerner and Smithgall, 2002) satisfactorily account for disease development and progression.

An important clue to the issue is that Nef predominantly localized to the Golgi apparatus (Greenberg et al., 1998; Drakesmith et al., 2005; Haller et al., 2007) and that Nef not only activated Hck but also induced skewed localization of Hck to the Golgi (Hung et al., 2007). The Golgi functions as a sorting hub and location of glycosylation for proteins, and several lines of evidence have revealed that Src kinases, shown to be involved in a wide array of intracellular signaling (reviewed in

Contract grant sponsor: Ministry of Education, Culture, Sports, Science and Technology of Japan.
Contract grant sponsor: Human Science Foundation, Japan.

*Correspondence to: Seiji Okada, Division of Hematopoiesis, Center for AIDS Research, Kumamoto University, Kumamoto 860-0811, Japan. E-mail: okadas@kumamoto-u.ac.jp

Received 17 February 2009; Accepted 11 June 2009

Published online in Wiley InterScience (www.interscience.wiley.com.), 7 July 2009.
DOI: 10.1002/jcp.21878

Lowell, 2004), also play a role in the regulation of the Golgi structure/function. First, a fraction of Src kinases, including Hck, is physiologically found at the Golgi (David-Pfeuty and Nouvian-Dooghe, 1990; Kaplan et al., 1992; Ley et al., 1994; Bijlmakers et al., 1997; van't Hof and Resh, 1997; Carreno et al., 2000; Kasahara et al., 2004). Second, fibroblasts lacking three ubiquitous Src kinases (c-Src/Yes/Fyn) exhibited an aberrant Golgi structure composed of collapsed stacks and bloated cisternae (Bard et al., 2003). Third, an increased protein load entering the *cis*-Golgi from the endoplasmic reticulum activated the Golgi-localized Src kinases, which in turn regulated overall protein trafficking activity in the secretory pathway (Pulvirenti et al., 2008). Importantly, the study by Pulvirenti et al. indicates that coordinated regulation of activity of the Golgi-localized Src kinases is crucial to maintain the Golgi function, which raises an intriguing possibility that Nef affects protein trafficking process and thereby macrophage phenotype/function through skewed Golgi-localization of active Hck.

Indeed, we recently identified an aberrant function of Nef, which was possibly due to the skewed Golgi-localization of active Hck. We previously found that Nef inhibited the signal of M-CSF, a primary cytokine for macrophages (Suzu et al., 2005), which was a possible trigger to worsen uncontrolled immune systems in patients, as M-CSF is essential to maintain macrophages at an anti-inflammatory state (reviewed in Hamilton, 2008). Of interest was the role of Hck in this inhibitory activity of Nef (Hiyoshi et al., 2008). Nef reduced cell surface expression of M-CSF receptor Fms in myeloid cells and macrophages, which was the direct cause of the inhibitory activity of Nef on M-CSF signal. Importantly, such reduced cell surface expression of Fms was reproduced in transfected 293 cells, but only in co-expression with Hck. More importantly, the reduced cell surface expression was due to the accumulation of an immature under-*N*-glycosylated Fms at the Golgi (hereinafter called Fms maturation arrest). However, constitutive-active Hck alone failed to induce such Fms maturation arrest. These results indicate that Nef inhibits M-CSF signal by arresting Fms *N*-glycosylation and trafficking at the Golgi and that such Fms maturation arrest was not caused just because of Hck activation. Thus, a most likely cause of Nef-induced Fms maturation arrest was skewed Golgi-localization of active Hck. However, this intriguing hypothesis should be carefully and directly tested, because it will not only help to clarify molecular basis of this novel function of Nef through Hck, but also provide an excellent example of disease-associated failure of the Golgi function regulation by the Golgi-localized Src kinases.

In this study, we therefore sought to definitely conclude that skewed Golgi-localization of active Hck was indeed the direct cause of Fms maturation arrest by Nef. To this end, we employed two different approaches. First, we prepared various Nef proteins and compared their abilities to induce skewed Golgi-localization of Hck, Hck activation and Fms maturation arrest. Second and importantly, we discovered a small-molecule non-kinase inhibitor that effectively blocked Nef-Hck binding and performed mechanistic analyses with the newly discovered compound.

Materials and Methods

Expression plasmids

For the expression in HEK293 cells (Invitrogen, Carlsbad, CA), human Fms- and human p56Hck cDNA cloned into pCDNA3.1 vector (Invitrogen) were used (Suzu et al., 2005; Hiyoshi et al., 2008). The constitutive-active Hck P2A mutant (Hiyoshi et al., 2008) was also used in selected experiments. The expression plasmid for human Lyn cloned in pME-puro vector was provided by Y. Yamanashi (Tokyo Medical and Dental University, Tokyo, Japan) and used in the pull-down assay with GST-Nef fusion proteins (see below). Nef cDNA derived from the NL43 or SF2 strain of HIV-1 was cloned into pRc/CMV-CD8 vector to express the extracellular/transmembrane regions of CD8-Nef fusion protein (Hiyoshi et al., 2008). NL43 Nef-M20A was prepared as described previously (Akari et al., 2000). NL43 Nef-AxxA and $-\Delta E$ mutant were provided by A. Adachi (University of Tokushima, Tokushima, Japan) and J.C. Guatelli (University of California, San Diego, CA), respectively. In this study, we prepared another NL43 Nef mutant (NL43 Nef-TR), by using QuikChange II Site-directed Mutagenesis Kits (Stratagene, La Jolla, CA). We also prepared Nef constructs expressing Nef-GFP fusion proteins (Ueno et al., 2008). For the expression of GST-Nef fusion proteins, fragments containing the entire coding sequences of the wild-type NL43 Nef, NL43 Nef-TR mutant, wild-type SF2 Nef, and SF2 Nef-AxxA mutant were subcloned into pGEX-6P-1 vector (GE Healthcare, Buckinghamshire, UK). SF2 Nef-AxxA mutant was prepared by using QuikChange II Site-directed Mutagenesis Kits (Stratagene). The nucleotide sequences of the coding region of all Nef constructs were verified by using BigDye Terminator v3.1 Cycle Sequencing Kit (Applied Biosystems, Foster City, CA) and ABI PRISM 3100 Genetic Analyzer (Applied Biosystems).

Chemicals

PP2 (Sigma, San Diego, CA) was used as the Src kinase inhibitor. UCS15A and its synthetic derivatives, 2b and 2c, were prepared as described (Oneyama et al., 2003). All these inhibitors were dissolved in dimethyl sulfoxide (DMSO; Wako, Osaka, Japan).

Western blotting

HEK293 cells were maintained with DME medium (Wako) supplemented with 10% fetal calf serum (FCS). The maturation of Fms proteins or the activation of Hck was analyzed by the transient expression assay with the cells followed by Western blotting as described previously (Suzu et al., 2005; Hiyoshi et al., 2008). In brief, cells grown on a 12-well tissue culture plate were transfected with plasmid for Fms (0.4 μg), Nef (0.8 μg), or Hck (0.4 μg) in the combinations indicated using LipofectAMINE2000 reagent (Invitrogen), unless otherwise stated. Total amounts of plasmids were normalized with the empty vectors. After 6 h, culture medium was replaced with complete medium and the transfected cells were cultured for an additional 42 h. In selected experiments, chemicals such as PP2 and 2c were added to the culture at the same time of changing medium. Total cell lysates were prepared essentially as described (Suzu et al., 2000). Primary antibodies used for Western blotting were as follows: anti-Fms (C-20; Santa Cruz Biotechnology, Santa Cruz, CA), anti-CD8 (H-160; Santa Cruz), anti-GFP (FL; Santa Cruz), anti-Hck (clone 18; Transduction Laboratories, Lexington, KY), anti-Hck phosphorylated at tyrosine 411 (Hck-pTyr^{411}; Santa Cruz), anti-phosphotyrosine (PY99; Santa Cruz), and anti-ERK1/2 (K-23; Santa Cruz). The relative intensity of bands on scanned gel images was quantified using NIH Image software, and the Fms maturation arrest or Hck activation is also shown graphically on an arbitrary unit. The relative intensity of bands on Hck-pTyr^{411} blots was quantified and the degree of Hck activation was expressed as a fold-increase relative to the control. For Fms maturation arrest, we calculated the percentage of immature under-*N*-glycosylated Fms of total Fms protein amount, and compared the percentages among samples.

Immunofluorescence

The signal of Nef-GFP was directly visualized with a BZ-8000 fluorescent microscope (Keyence, Osaka, Japan) equipped with Plan-Fluor ELWD 20x/0.45 objective lenses (Nikon, Tokyo, Japan) (Hiyoshi et al., 2008). To detect active Hck, cells were fixed in 2% paraformaldehyde, permeabilized with ethanol, and stained with goat anti-active Hck antibodies (Santa Cruz). Secondary antibodies were anti-goat IgG-AlexaFluo488 (Molecular Probes, Eugene, OR). Nuclei were stained with DAPI (Molecular Probes), and

fluorescent signals were visualized as above. Image processing was performed using BZ-analyzer (Keyence) and Adobe Photoshop Software (Adobe Systems, San Jose, CA).

GST pull-down

The control GST or GST-Nef fusion proteins (wild-type NL43 Nef, NL43 Nef-TR, wild-type SF2 Nef, and SF2 Nef-AxxA) cloned in pGEX-6P-1 vector was expressed in *E. coli* BL21 cells (GE Healthcare). Cells were grown in LB media containing 50 μg/ml ampicillin followed by induction with 1 μM IPTG. The expression-induced cells were harvested and lysed with BugBuster Protein Extraction Reagent containing 1 U/ml rLysozyme and 25 U/ml Benzonaze Nuclease (Novagen, Madison, WI). The cleared lysates were then incubated with GST-Bind Resin (Novagen). After extensive washing with GST Bind/Wash Buffer (Novagen), the resin was incubated with the total cell lysates of HEK293 cells transfected with the expression plasmid for Hck or Lyn. In a selected experiment, 2c was added to the mixtures. After extensive re-washing, the resin was boiled with SDS–PAGE sample buffer and elutes were analyzed for the presence of Hck or Lyn by western blotting. Primary antibodies used were as follows (both from Transduction Laboratories): anti-Hck (clone 18) and anti-Lyn (clone 42). In a selected experiment, we also used GST proteins fused to the SH3 domain of Hck (Paliwal et al., 2007), which was provided by G. Swarup (Center for Cellular and Molecular Biology, Hyderabad, India).

Subcellular fractionation

The subcellular fractionation on sucrose gradients was performed exactly as reported (Matsuda et al., 2006). In brief, cells were

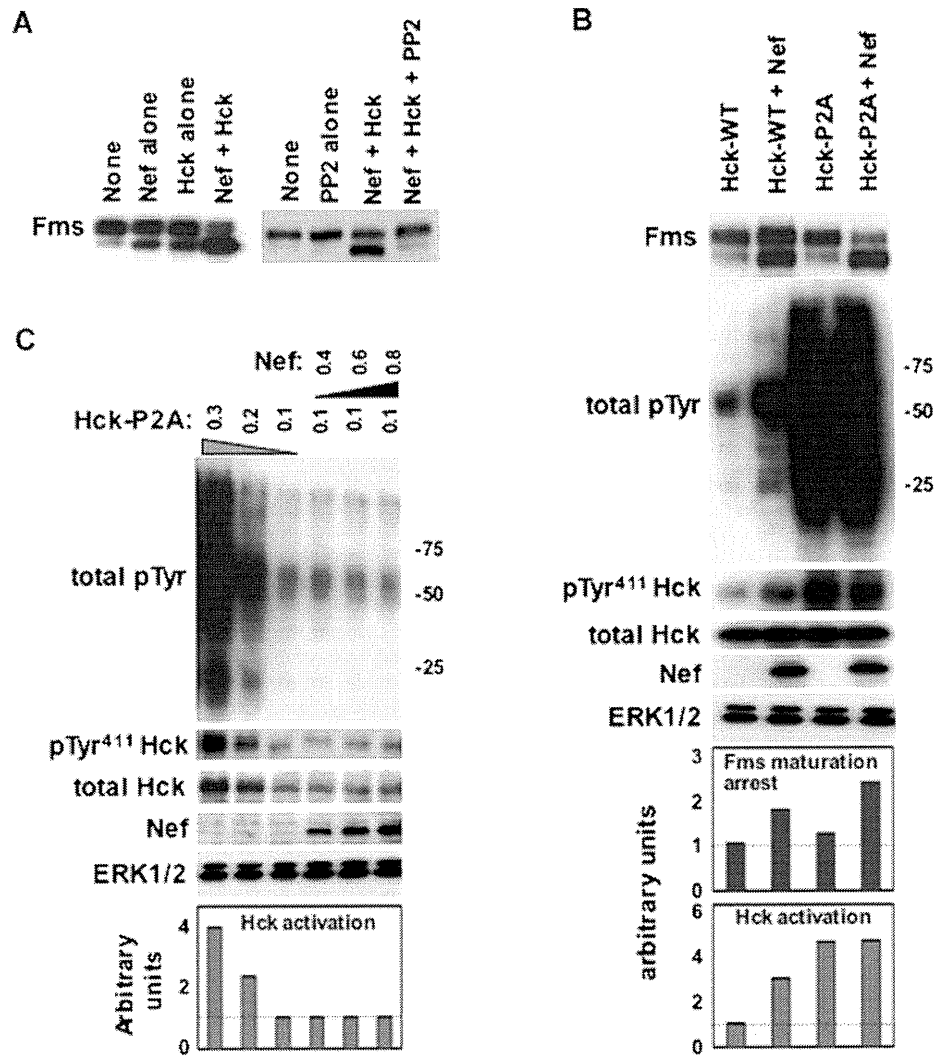

Fig. 1. Nef/Hck-induced Fms mturation arrest. A: HEK293 cells were transfected with Fms plamid alone (None) or co-transfected with the plasmids for NL43 Nef and/or wild-type Hck as indicated. In the right blot, PP2 was added to selected wells at a final concentration of 10 μM after the transfection, Total cell lysates were subjected to Fms Western blotting. B: Cells were transfected with Fms plasmid alone (None) or in combination with the plasmids for Nef (NL43) and Hck (WT or constitutive-active P2A), as indicated. These cells were then analyzed for the expression of Fms, tyrosine-phosphorylated proteins (total pTyr), active-Hck (pTyr^{411}Hck), total Hck, CD8-Nef (Nef), or ERK by Western blotting. The ERK blot is a loading control. The quantified Fms maturation arrest and Hck activation are shown in the bar graphs. C: Cells were transfected with varying amounts (μg) of Hck-P2A and NL43 Nef plasmids as indicated, and analyzed as in (B). The quantified Hck activation is shown in the bar graphs. [Color figure can be viewed in the online issue, which is available at www.interscience.wiley.com.]

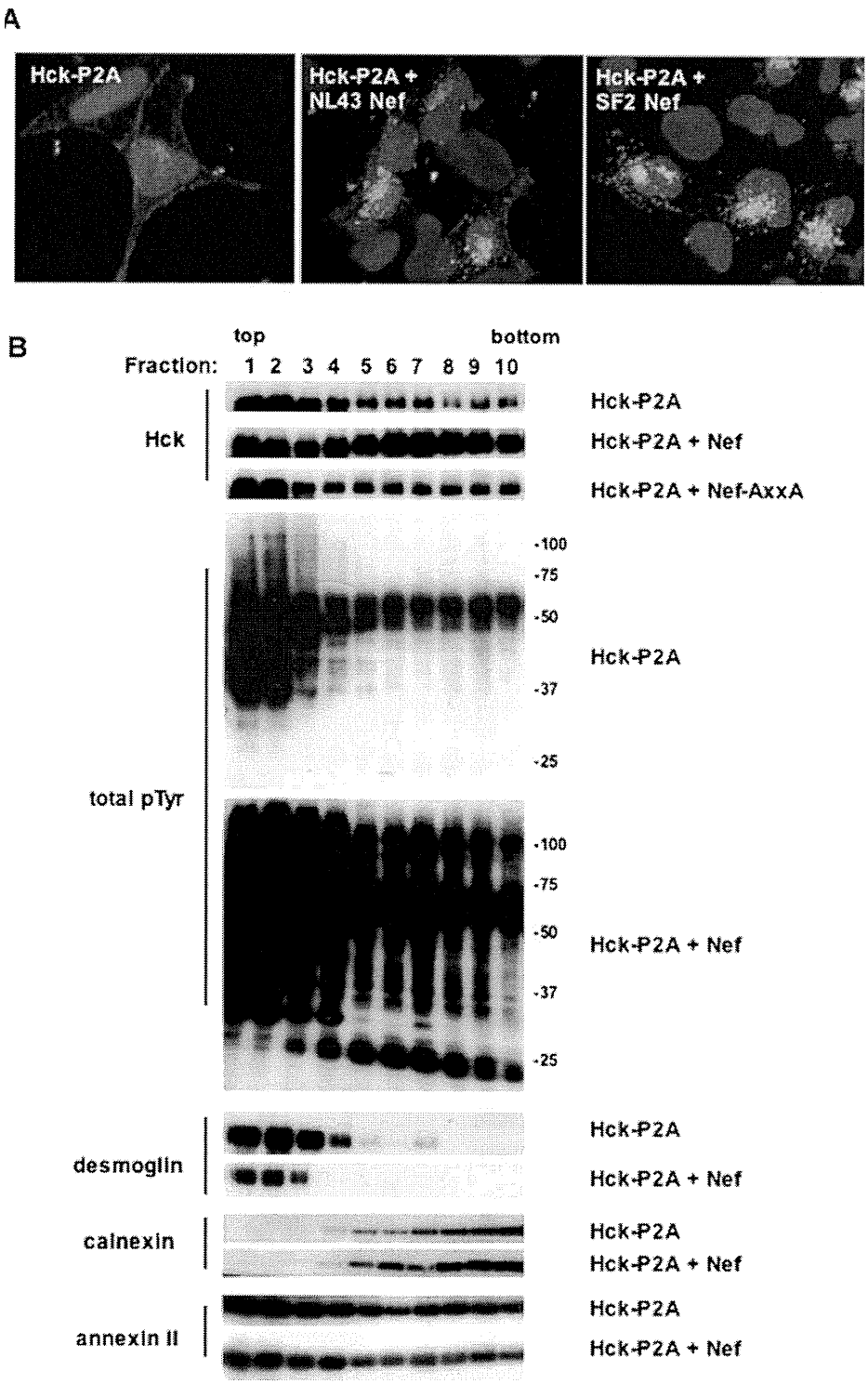

Fig. 2. Skewed Golgi-localization of Hck by Nef. A: HEK293 cells were transfected with Hck-P2A plasmid alone, or co-transfected with NL43 Nef or SF2 Nef plasmid. Cells were stained with antibody specific for active Hck (green) and DAPI (blue). B: Cells were transfected with Hck-P2A alone, or co-transfected with NL43 Nef. Then, cells were subjected to subcellular fractionation on sucrose gradients and Western blotting with antibodies against Hck, phosphotyrosine (pTyr), desmoglein, calnexin, or annexin II. [Color figure can be viewed in the online issue, which is available at www.interscience.wiley.com.]

swollen in hypotonic buffer containing protease inhibitors followed by homogenization. Then, the post-nuclear supernatants were fractionated by ultracentrifugation on discontinuous sucrose gradients. All steps were carried out on ice. The fractions obtained were subjected to Western blotting with antibodies to Hck (clone 18; Transduction Laboratories), desmoglein (clone 62; Transduction Laboratories), annexin II (C-10; Santa Cruz), or calnexin (H-70; Santa Cruz).

Flow cytometry

Human myeloid TF-1-fms cells expressing Nef-ER fusion protein were maintained as described previously (Suzu et al., 2005; Hiyoshi et al., 2008). To activate the Nef-ER fusion protein, we used the estrogen analog 4-HT (Sigma) at a final concentration of 0.1 μM. The cells were stained with PE-labeled anti-Fms antibodies (Santa Cruz), and the level of cell surface Fms was analyzed by flow cytometry on a FACS Calibur using Cell Quest software (Becton Dickinson, Mountain View, CA).

Results

Analyses with Src kinase inhibitor and Hck mutant

As reported, Nef induces Fms maturation arrest when co-expressed with Hck in HEK293 cells (Fig. 1A). HEK293 cells do not express Hck endogenously, and the upper and lower band was the fully *N*-glycosylated and under-*N*-glycosylated Fms, respectively (Hiyoshi et al., 2008). The low molecular weight Fms was sensitive to Endo-H (Endo-β-*N*-acetylglucosaminindase H), which selectively cleaves high-mannose type oligosaccharide, and their increase was clearly associated with the intense staining of Fms mainly at

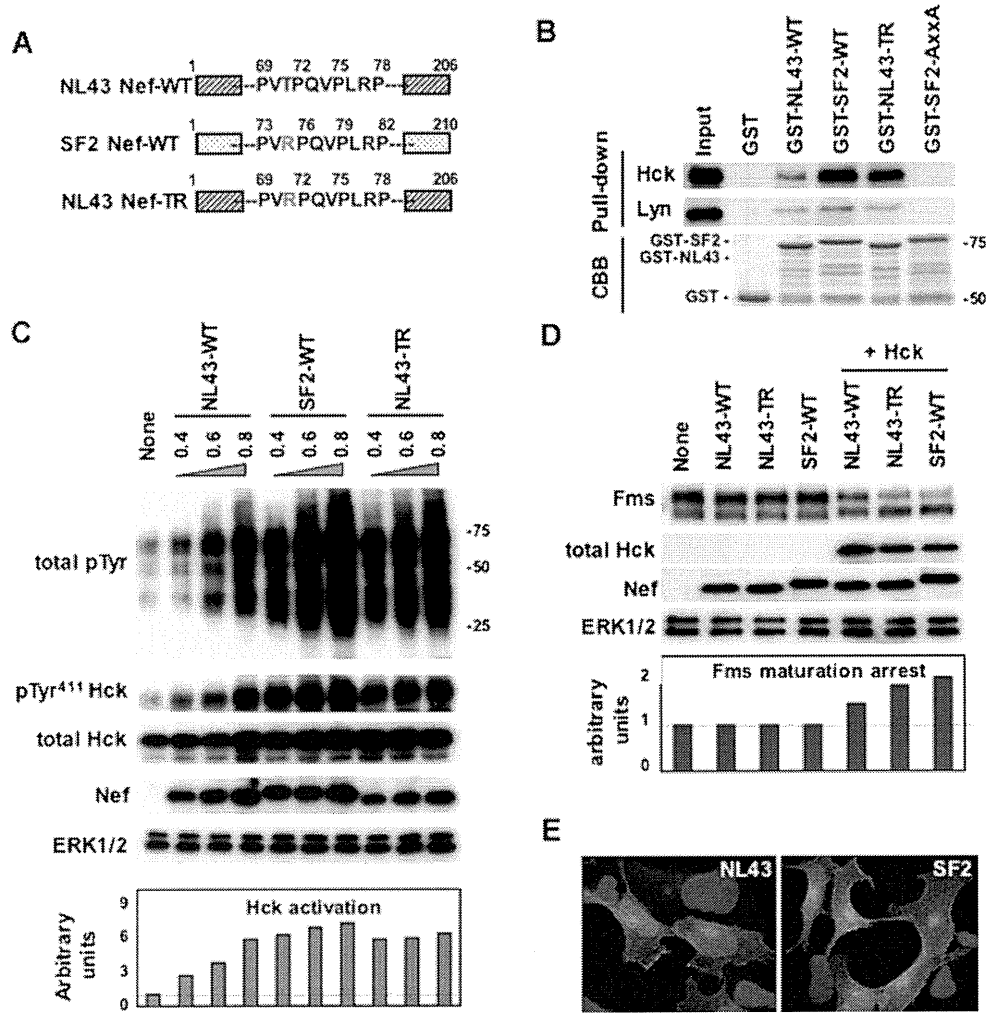

Fig. 3. Abilities of different Nef alleles to bind/activate Hck and to induce Fms maturation arrest. A: The NL43 Nef, SF2 Nef, and NL43 Nef-TR mutant used are schematically shown. B: The resins, to which the control GST or indicated GST-Nef proteins were bound, were incubated with the lysates of HEK293 cells expressing Hck or Lyn. The amount of Hck or Lyn bound to the resins was determined by Western blotting (Pull-down). The amount of GST and GST-Nef fusion proteins bound to the resins was verified by the elution from the resins followed by SDS–PAGE/Coomassie brilliant blue (CBB) staining. C: HEK293 cells were co-transfected with the wild-type Hck and indicated Nef alleles. The amounts of Nef plasmids used are shown (0.4, 0.6, or 0.8 μg/well). Total cell lysates were subjected to Western blotting with antibodies against phosphotyrosine (total pTyr), active-Hck (pTyr^{411} Hck), total Hck, CD8-Nef (Nef), or ERK by Western blotting. The quantified Hck activation is shown in the bar graph. D: Cells were transfected with Fms plasmid alone (None) or in combination with the plasmids for Nef and Hck, as indicated. Western blotting was done as in (C). E: Cells were transfected with indicated GFP-Nef plasmid (green). Nuclei were stained with DAPI (blue). [Color figure can be viewed in the online issue, which is available at www.interscience.wiley.com.]

the perinuclear region, which overlapped well with the signal of GM130 or Vti1a, the markers for the Golgi (Hiyoshi et al., 2008). These results strongly suggested that the low molecular weight Fms was the immature under-*N*-glycosylated form. The increase of the lower molecular weight species was obvious in the cells co-expressing Nef and Hck (Fig. 1A, left blot), and this Fms maturation arrest was blocked by a Src kinase inhibitor PP2 (Fig. 1A, right blot). However, the expression of a constitutive-active Hck mutant (Hck-P2A; Lerner and Smithgall, 2002) was not sufficient to induce Fms maturation arrest when expressed alone (Fig. 1B, Fms blot), despite its strong kinase activity (total pTyr and $pTyr^{411}$ Hck blots). In this study, we monitored kinase activity of Hck by overall protein tyrosine-phosphorylation (total pTyr) and auto-phosphorylation of Hck ($pTyr^{411}$ Hck) (reviewed in Korade-Mirnics and Corey, 2000). Nonetheless, Hck-P2A/Nef co-expression induced more severe Fms maturation arrest than wild-type Hck/Nef co-expression (Fig. 1B), and Nef did not enhance the kinase activity of Hck-P2A (Fig. 1C), confirming our previous finding that Hck activation was necessary but not sufficient for Nef-induced Fms maturation arrest.

Analyses with different Nef alleles and their mutants

In this study, we first found that Nef derived from SF2 strain of HIV-1 induced more severe Golgi-localization of Hck-P2A than Nef derived from NL43 strain. Hck-P2A signal at the plasma membrane was still observed in some NL43 Nef-transfected cells, whereas such signal was not observed in SF2 Nef-transfected cells (Fig. 2A). The Nef-induced skewed Golgi-localization of Hck-2PA was confirmed by a quantitative analysis, that is, subcellular fractionation on sucrose gradients. Based on a previous report (Matsuda et al., 2006), we used desmoglein, annexin II and calnexin as marker proteins for the plasma membrane, both the plasma membrane and the Golgi, and the endoplasmic reticulum, respectively. As shown (Fig. 2B), the plasma membrane was recovered in light fractions whereas the Golgi and the endoplasmic reticulum were recovered in heavy fractions, and the peak of Hck-P2A shifted to heavy fractions by the co-expression with NL43 Nef but not a Nef-AxxA mutant defective in the binding to Hck (Saksela et al., 1995). The peak shift was also associated with the appearance of many tyrosine-phosphorylated proteins in these fractions (Fig. 2B).

Both NL43 Nef and SF2 Nef had intact PxxP motif (Fig. 3A), but SF2 Nef showed much higher affinity to Hck than NL43 Nef (Fig. 3B). In the control experiments, we confirmed that the binding of both Nef to Lyn remained low and the PxxP motif-disrupted SF2 Nef mutant (AxxA) bound neither Hck nor Lyn. Reflecting the higher affinity to Hck, SF2 Nef induced stronger Hck activation (Fig. 3C) and more severe Fms maturation arrest (Fig. 3D). As expected, even SF2 Nef failed to induce Fms maturation arrest when co-expressed with Lyn (data not shown). However, SF2 Nef and NL43 Nef showed no obvious change in the pattern of predominant Golgi-localization (Fig. 3E). It was therefore likely that SF2 Nef bound Hck at

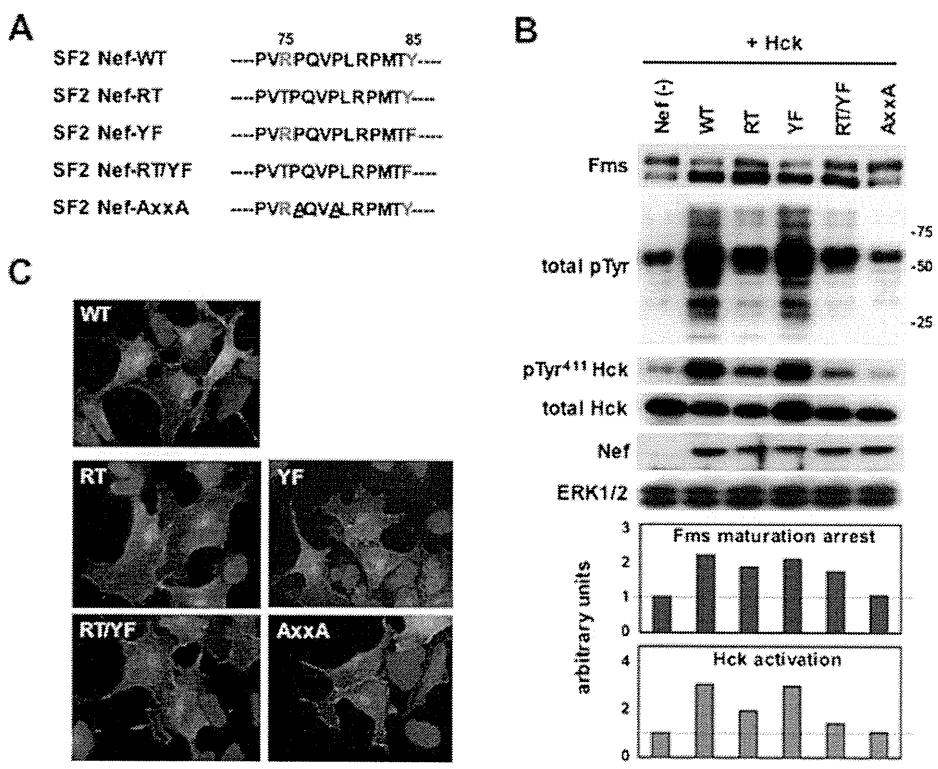

Fig. 4. Abilities of SF2 Nef mutants to activate Hck and to induce Fms maturation arrest. A: The SF2 Nef mutants used (RT, YF, RT/YF, and AxxA) are schematically shown. B: HEK293 cells were transfected with Fms plasmid alone (None) or in combination with the plasmids for Nef and Hck, as indicated. These cells were then analyzed for the expression of Fms, phosphotyrosine (total pTyr), active-Hck ($pTyr^{411}$Hck), total Hck, GFP-Nef (Nef), or ERK by Western blotting. The quantified Fms maturation arrest and Hck activation are shown in the bar graphs. C: Cells were transfected with indicated GFP-Nef plasmid (green). Nuclei were stained with DAPI (blue). [Color figure can be viewed in the online issue, which is available at www.interscience.wiley.com.]

the Golgi with higher affinity and thereby induced stronger Hck activation and more severe Fms maturation arrest.

There was a single amino acid difference within the PxxP motif, Thr^{71} in NL43 Nef and Arg^{75} in SF2 Nef (Fig. 3A). We found that an NL43 Nef with $Thr^{71}Arg$ substitution (NL43 Nef-TR) showed higher affinity to Hck than wild-type NL43 Nef (Fig. 3B), and induced stronger Hck activation (Fig. 3C) and more severe Fms maturation arrest (Fig. 3D) than wild-type NL43 Nef. We also performed a complementary experiment with SF2 Nef mutants (Fig. 4A; Ueno et al., 2008). As a result, we found that mutants with $Arg^{75}Thr$ substitution (SF2 Nef-RT and SF2-RT/YF) induced moderate Hck activation/Fms maturation arrest (Fig. 4B). However, both showed no obvious change in the pattern of predominant Golgi-localization (Fig. 4C). These results indicated that the single amino acid difference (Thr to Arg) within the PxxP motif governed the higher ability of SF2 Nef to induce Golgi-localization and activation of Hck, and Fms maturation arrest.

Although PxxP motif is essential for Nef to bind Hck, a recent study showed that an acidic region of Nef facilitated Nef-Hck binding at the Golgi (Hung et al., 2007). Although an NL43 Nef mutant lacking this region (ΔE; Fig. 5A) bound GST-Hck SH3 fusion proteins as with wild-type NL43 Nef (Fig. 5B), ΔE mutant was indeed less active than wild-type in transfected HEK293 cells, that is, in both Hck and activation Fms maturation arrest (Fig. 5C). Another mutant (M20; Fig. 5A), which was defective in the down-regulation of MHC I, another hallmark function of Nef (Akari et al., 2000), retained the ability to induce Hck activation and Fms maturation arrest (Fig. 5C). Both ΔE and M20A mutants showed no obvious change in the pattern of predominant Golgi-localization (Fig. 5C). The result further supported the idea that stronger Hck activation, which took place at the Golgi, induced severe Fms maturation arrest.

Analyses with a newly discovered Nef-Hck binding blocker

To directly show that the Golgi-localization of active Hck determines Nef-induced Fms maturation arrest, we sought to discover Nef-Hck binding blockers. In this study, we focused on UCS15A and its analogs 2b and 2c (Fig. 6A), because these small-molecule compounds were shown to block several proline-rich motif-SH3 domain binding such as Sam68-Fyn binding (Oneyama et al., 2003) and AMAP1-cortactin binding (Hashimoto et al., 2006). As they have not been used before for HIV-1 studies, we tested their capability to block Nef-Hck binding by the GST pull-down assay. As shown (Fig. 6B), all compounds blocked the binding of Hck to NL43 Nef or NL43 Nef-TR mutant (more potent than the wild-type, see Fig. 3), in a dose-dependent manner. Like the case of Sam68-Fyn binding (Oneyama et al., 2003), 2c was the most effective in blocking Nef-Hck binding (Fig. 6B), and showed no obvious toxicity to HEK293 cells (Fig. 6C). As shown (Fig. 6D), 2c indeed inhibited

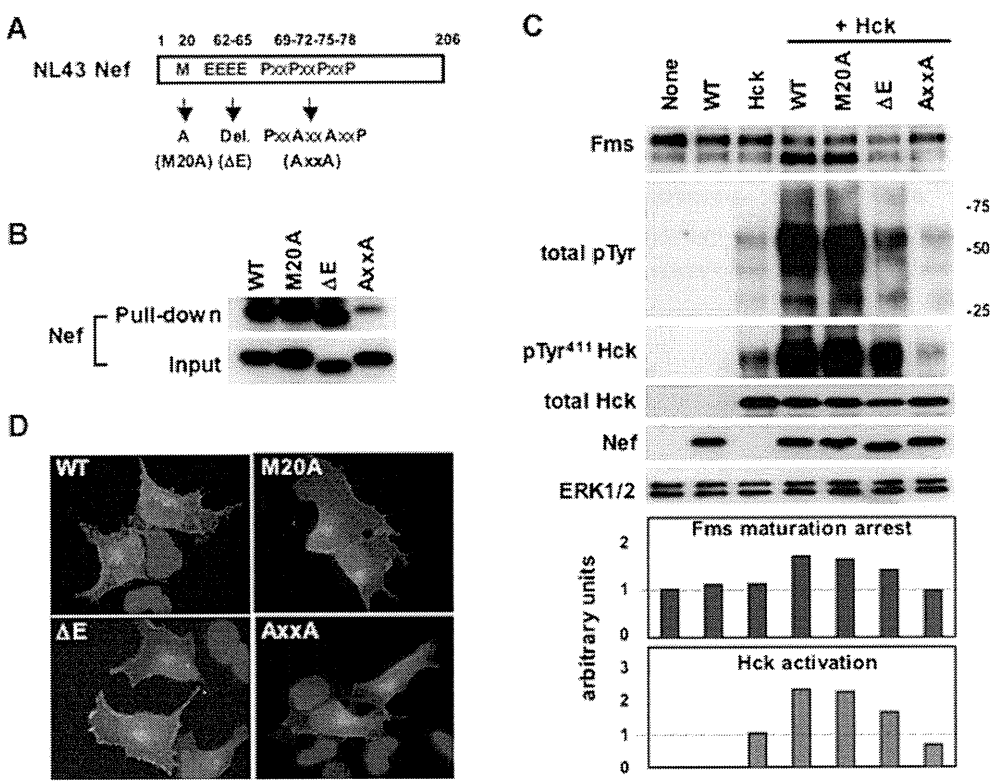

Fig. 5. Abilities of NL43 Nef mutants to activate Hck and to induce Fms maturation arrest. A: The NL43 Nef mutants used (M20A, ΔE, and AxxA) are schematically shown. B: The resin, to which GST-Hck SH3 fusion proteins were bound, were incubated with the lysates of HEK293 cells expressing the indicated Nef proteins. The amount of Nef proteins in the lysates (Input) or bound to the resins (Pull-down) was verified by Western blotting. C: HEK293 cells were transfected with Fms plasmid alone (None) or in combination with the plasmids for Nef and Hck, as indicated. These cells were then analyzed for the expression of Fms, phosphotyrosine (total pTyr), active-Hck ($pTyr^{411}$ Hck), total Hck, CD8-Nef (Nef), or ERK by Western blotting. The quantified Fms maturation arrest and Hck activation are shown in the bar graphs. D: Cells were transfected with indicated GFP-Nef (green). Nuclei were stained with DAPI (blue). [Color figure can be viewed in the online issue, which is available at www.interscience.wiley.com.]

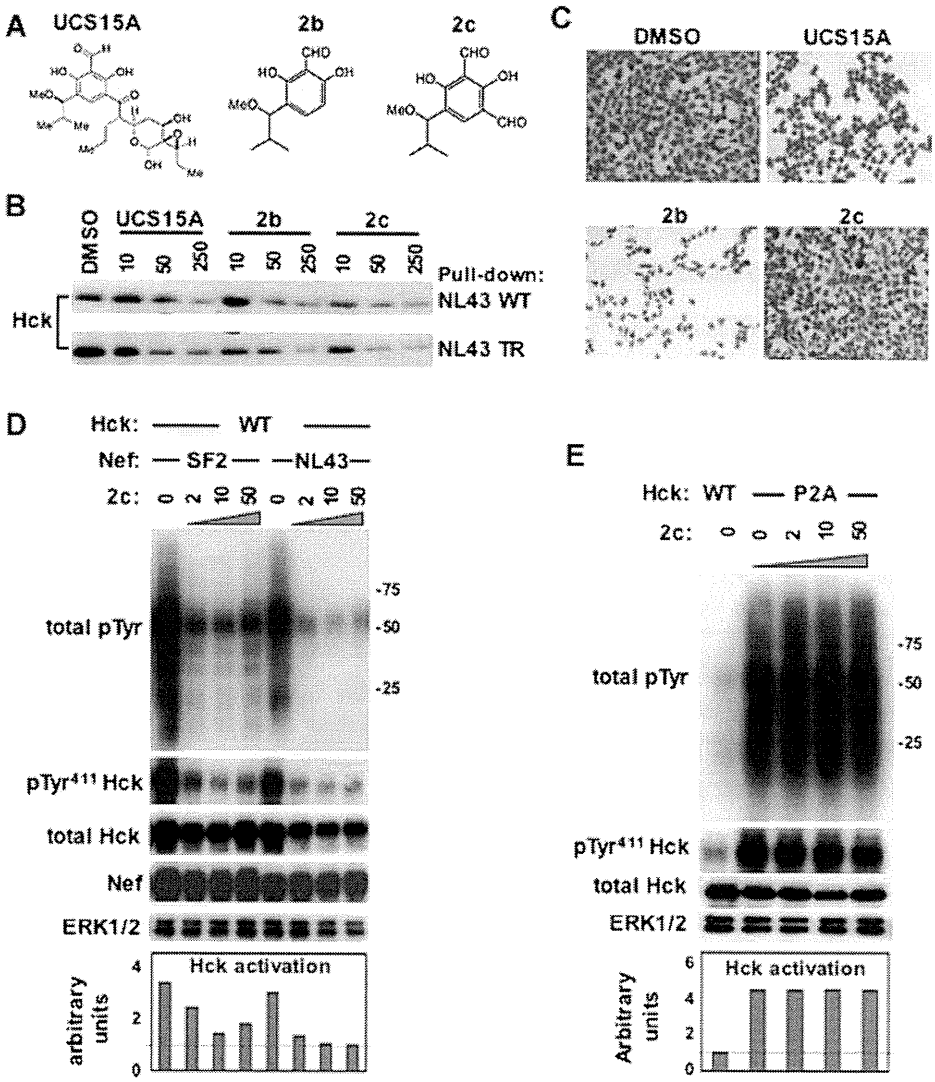

Fig. 6. Capability of 2c to block Nef-Hck binding and Nef-induced Hck activation. A: Chemical structures of UCS15A, 2b, and 2c are shown. B: The resins, to which GST-Nef (NL43 wild-type or TR mutant, see Fig. 2A) proteins were bound, were incubated with the lysates of Hck-expressing HEK293 cells in the absence (DMSO) or presence of the indicated concentration (0, 10, 50, or 250 μM) of UCS15A, 2b, or 2c. The amount of Hck proteins bound to the resins was determined by Western blotting. C: HEK293 cells were cultured in the absence (DMSO) or presence of 50 μM of UCS15A, 2b, or 2c for 2 days, and subjected to Wright-Giemsa staining. D: Cells were co-transfected with Hck-WT and indicated Nef alleles (SF2 or NL43), and cultured in the presence of increasing concentrations (μM) of 2c. These cells were then analyzed for the expression of tyrosine-phosphorylated proteins (total pTyr), active-Hck (pTyr^{411}Hck), total Hck, CD8-Nef (Nef), or ERK by Western blotting. The quantified Hck activation is shown in the bar graphs. E: Cells were transfected with Hck-WT or Hck-P2A, and cultured in the presence of increasing concentrations (μM) of 2c. These cells were analyzed as in (D). [Color figure can be viewed in the online issue, which is available at www.interscience.wiley.com.]

Hck activation by NL43 Nef and more potent SF2 Nef (see Fig. 3). Importantly, 2c had little inhibitory effect on kinase activity of the constitutive-active Hck P2A mutant, even when used at a concentration as high as 50 μM (Fig. 6E). These results indicated that 2c was not a kinase inhibitor but inhibited Nef-induced Hck activation by blocking Nef-Hck binding.

This unique feature of 2c prompted us to examine whether 2c blocks Nef/Hck-induced Fms maturation arrest and Nef-induced skewed Golgi-localization of Hck. As shown (Fig. 7A), 2c completely blocked Fms maturation arrest induced by Nef and wild-type Hck as expected. However, of particular importance was that 2c also completely blocked severe Fms maturation arrest induced by Nef and the constitutive-active Hck P2A (Fig. 7B). Because 2c had little inhibitory effect on kinase activity of Hck-P2A (see Fig. 6E), these results strongly supported that the presence of Hck-P2A at the Golgi caused by its binding with Nef (see Fig. 2) was a direct cause of severe Fms maturation arrest. We therefore sought to verify that 2c indeed blocked Nef-induced skewed Golgi-localization of Hck-P2A. To this end, we employed the quantitative analysis, that is, subcellular fractionation on sucrose gradients (see Fig. 2B). The peak of Hck-P2A shifted to heavier fractions by the co-expression with Nef, and such change in the intracellular localization of Hck-P2A was restored to normal by the addition of 2c (Fig. 7C). We also tested whether 2c blocked Nef-induced Fms abnormality in another culture system. We previously showed that the cell surface expression of Fms was impaired in human myeloid TF-1-fms cells expressing a conditionally active

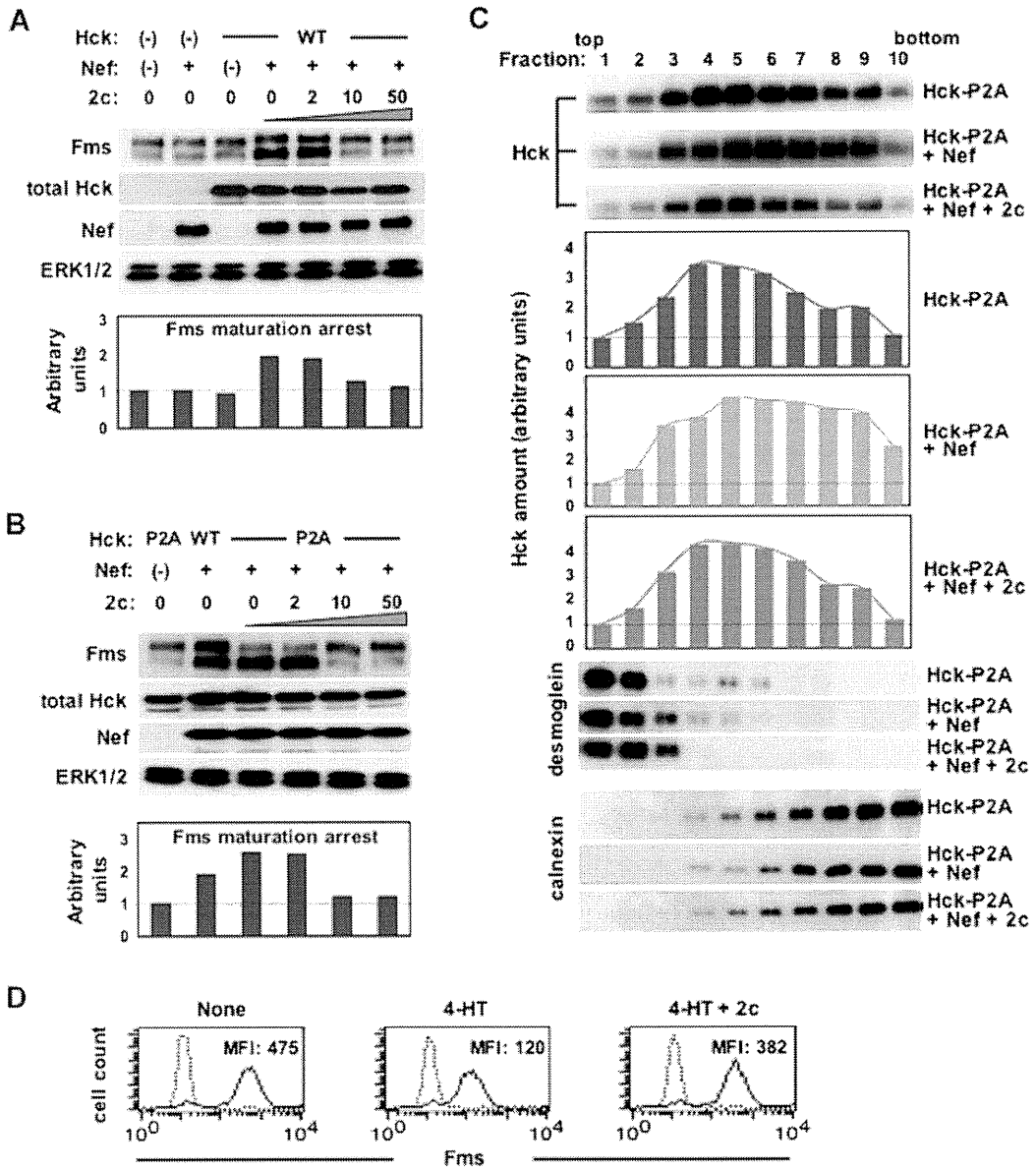

Fig. 7. Capability of 2c to block Fms maturation arrest and skewed Golgi-localization of Hck. A: HEK293 cells were transfected with the plasmids (Fms, NL43 Nef, and Hck-WT) in combination indicated, and cultured in the presence of increasing concentrations (μM) of 2c. These cells were then analyzed for the expression of Fms, total Hck, CD8-Nef (Nef), or ERK by Western blotting. The quantified Fms maturation arrest is shown in the bar graphs. B: Cells were transfected with the plasmids (Fms, NL43 Nef, Hck-WT, and Hck-P2A) in combination indicated, and cultured in the presence of increasing concentrations (μM) of 2c. These cells were then analyzed as in A. C: Cells were transfected with Hck-P2A alone (top), or co-transfected with NL43 Nef (middle). 2c was added to a final concentration of 50 μM to selected wells (bottom). Then, cells were subjected to subcellular fractionation on sucrose gradients and Hck Western blotting. The quantified Hck amounts are shown in the bar graph. The fractions were also analyzed for the amount of desmoglein and calnexin. D: TF-1-fms-Nef-ER cells cultured with M-CSF-free media in the absence (left) or presence of 0.1 μM 4-HT (middle), or the co-presence of 0.1 μM 4-HT and 50 μM 2c (right) for 12 h. The expression of Fms on the surface of treated cells was analyzed by flow cytometry with PE-labeled anti-Fms. The mean fluorescence intensity (MFI) of Fms expression is indicated. [Color figure can be viewed in the online issue, which is available at www.interscience.wiley.com.]

Nef-ER fusion protein when the Nef-ER in the cells was activated by the estrogen analog 4-HT (Hiyoshi et al., 2008). This impaired cell surface Fms expression was highly likely due to intracellular Fms maturation arrest (Hiyoshi et al., 2008). Finally, we found that the Fms down-regulation in Nef-active TF-1-fms-Nef-ER cells was also restored to normal by the addition of 2c (Fig. 7D). All taken together, our present study clearly demonstrated that skewed Golgi-localization of active Hck induced by Nef was indeed the direct cause of Fms maturation arrest.

Discussion

M-CSF is a cytokine essential not only for the survival of macrophages but also for the maintenance of macrophages at an

anti-inflammatory state (reviewed in Chitu and Stanley, 2006; Hamilton, 2008). Thus, the inhibitory effect of Nef on M-CSF signal through Fms maturation arrest at the Golgi is a possible trigger to worsen uncontrolled immune systems in patients (Suzu et al., 2005; Hiyoshi et al., 2008). In this study, we therefore sought to define molecular basis of this important function of Nef, by using different Nef alleles, various Nef mutants, constitutive-active Hck mutant, and Nef-Hck binding blocker 2c. The study with various Nef proteins supported the idea that high affinity Nef-Hck binding and subsequent stronger Hck activation, both of which took place mainly at the Golgi, determined Fms maturation arrest at the Golgi (Figs. 2–5). Moreover, the study with 2c enabled us to conclude that skewed Golgi-localization of active Hck by Nef was indeed the direct cause of Fms maturation arrest (Figs. 6 and 7). By analogy with the Sam68-Fyn binding inhibition (Oneyama et al., 2003), the inhibitory effect of 2c on Nef-Hck binding was supposed to be mediated by its interaction with Nef PxxP motif.

As mentioned earlier, it has been known for a long time that most members of Src kinases including Hck localize to the Golgi as well as to the plasma membrane. For example, it was shown that newly synthesized Lyn initially localized and accumulated to the Golgi, and then moved toward the plasma membrane (Kasahara et al., 2004). Importantly, Pulvirenti et al. (2008) recently revealed that coordinated regulation of activity of the Golgi-localized Src kinases is crucial to maintain intra-Golgi trafficking of proteins. Our present finding that skewed Golgi-localization of active Hck leads to Fms maturation arrest at the Golgi is in line with the new concept. It appears that long-lasting and dys-regulated activation of the Golgi-localized Src kinases disturbs glycosylation and/or trafficking of proteins, exemplified by Fms maturation arrest. Indeed, N-Src, a c-Src isoform with a higher basal tyrosine kinase activity (Brugge et al., 1985), showed more obvious perinuclear localization than the constitutive-active Hck-P2A and induced Fms maturation arrest even in the absence of Nef (unpublished result). Moreover, Mitina et al. (2007) reported that over-expression of an active form of Hck disturbed *N*-glycosylation of another cytokine receptor Flt3 even in the absence of Nef. These results may further support the idea that long-lasting and dys-regulated activation of the Golgi-localized Src kinases per se affects protein glycosylation and/or trafficking at the Golgi. Anyhow, our system with Nef provides a useful model to elucidate how Src kinases regulate the Golgi structure/function. It will be important to identify which Golgi proteins are phosphorylated directly or indirectly by Hck activated at the Golgi and to clarify how such phosphorylation cascade leads to Nef-induced Fms maturation arrest.

Nef has been shown to affect protein trafficking and a well-characterized target is major histocompatibility complex class I (MHC I). Nef reduced the cell surface expression of MHC I, which diminishes the recognition of infected cells by cytotoxic T cells (reviewed in Fackler and Baur, 2002; Peterlin and Trono, 2003). However, it is still in intense debate whether Nef requires SH3 domain-containing proteins such as Hck to reduce the cell surface level of MHC I (Schwartz et al., 1996; Greenberg et al., 1998; Mangasarian et al., 1999; Akari et al., 2000; Chang et al., 2001; Roeth and Collins, 2006; Hung et al., 2007; Atkins et al., 2008). In this regard, Fms is not the direct target of Nef. However, as shown, Nef disturbed the cell surface expression of Fms, which is triggered by skewed Golgi-localization of active Hck. Moreover, it was shown that Nef disturbed the cell surface expression of another macrophage-specific protein HFE, an iron homeostasis regulator, which was blocked by a dominant-negative Hck (Drakesmith et al., 2005). Although whether the reduced cell surface level of HFE by Nef relates to skewed Golgi-localization of active Hck is unclear, it is conceivable that Nef acquires an additional machinery to manipulate protein trafficking in macrophages by exploiting the Golgi-localized Hck. Of interest, the *N*-glycosylation of Flt3, which is structurally related to Fms, was also impaired in Nef/Hck-expressing HEK293 cells, but the degree of maturation arrest of Flt3 was quite weak when compared to that of Fms (data not shown). The finding may imply that Fms maturation arrest is not necessarily due to the general disruption in the Golgi structure or function. Future studies, in which we determine to what extent overall protein *N*-glycosylation and trafficking are affected by Nef-Hck binding, will further clarify pathological significance of the molecular binding in macrophages. The newly discovered Nef-Hck binding blocker 2c will be useful in such studies and may provide a strategy to complement current anti-HIV-1 therapy for better treatment outcomes.

In this study, we showed that SF2 Nef had much higher affinity to Hck than NL43 Nef and thereby induced stronger Hck activation/severe Golgi-localization of Hck (Figs. 2 and 3) and that the single amino acid difference (Thr^{71} in NL43 Nef and Arg^{75} in SF2 Nef) within PxxP motif largely governs the higher ability of SF2 Nef (Figs. 3 and 4). This difference might reflect that the $Thr^{71}Arg$ substitution in NL43 Nef (NL43 Nef-TR, see Fig. 3) altered the flexibility of a loop containing the PxxP motif (Fackler et al., 2001). Importantly, for reasons not clearly understood, NL43 Nef-TR was more pathogenic in HIV-1 Tg mice than wild-type NL43 Nef and the pathogenicity of SF2 Nef in Tg mice was evident despite very low levels of expression (Priceputu et al., 2007). It is therefore possible that more severe Golgi-localization of active Hck followed by perturbed *N*-glycosylation and trafficking of proteins including Fms account for the high pathogenicity of SF2 Nef in Tg mice.

In summary, our present study clearly demonstrated that skewed Golgi-localization of active Hck was the direct cause of Fms maturation arrest by Nef. Our findings establishes an intriguing link between the pathogenesis of HIV-1 Nef and the newly emerging concept that the Golgi-localized Src kinases regulate the Golgi function. The identification of Golgi proteins phosphorylated by the Golgi-localized active Hck will provide novel insights into molecular mechanisms by which Nef functions as an HIV-1 pathogenetic factor through Hck and the Gogi-localized Src kinases regulate the Golgi function.

Acknowledgments

We thank Dr. G. Thomas (Vollum Institute) for critical reading of the manuscript. We thank Ms. Y. Endo and Ms. I. Suzu for experimental assistance.

Literature Cited

Akari H, Arold S, Fukumori T, Okazaki T, Strebel K, Adachi A. 2000. Nef-induced major histocompatibility complex class I down-regulation is functionally dissociated from its virion incorporation, enhancement of viral infectivity, and CD4 down-regulation. J Virol 74:2907–2912.

Arold S, O'Brien R, Franken P, Strub MP, Hoh F, Dumas C, Ladbury JE. 1998. RT loop flexibility enhances the specificity of Src family SH3 domains for HIV-1 Nef. Biochemistry 37:14683–14691.

Atkins KM, Thomas L, Youker RT, Harriff MJ, Pissani F, You H, Thomas G. 2008. HIV-1 Nef binds PACS-2 to assemble a multikinase cascade that triggers major histocompatibility complex class I (MHC-I) down-regulation: Analysis using short interfering RNA and knock-out mice. J Biol Chem 283:11772–11784.

Bard F, Mazelin L, Pechoux-Longin C, Malhotra V, Jurdic P. 2003. Src regulates Golgi structure and KDEL receptor-dependent retrograde transport to the endoplasmic reticulum. J Biol Chem 278:46601–46606.

Bijlmakers MJ, Isobe-Nakamura M, Ruddock LJ, Marsh M. 1997. Intrinsic signals in the unique domain target p56lck to the plasma membrane independently of CD4. J Cell Biol 137:1029–1040.

Brugge JS, Cotton PC, Queral AE, Barrett JN, Nonner D, Keane RW. 1985. Neurones express high lenels of a structurally modified, activated form of pp60c-src. Nature 316:554–557.

Carreno S, Gouze ME, Schaak S, Emorine LJ, Maridonneau-Parini I. 2000. Lack of palmitoylation redirects $p59^{Hck}$ from the plasma membrane to $p61^{Hck}$-positive lysosomes. J Biol Chem 275:36223–36229.

Chang AH, O'Shaughnessy MV, Jirik FR. 2001. Hck SH3 domain-dependent abrogation of Nef-induced class I MHC down-regulation. Eur J Immunol 31:2382–2387.

Chitu V, Stanley ER. 2006. Colony-stimulating factor-1 in immunity and inflammation. Curr Opin Immunol 18:39–48.

David-Pfeuty T, Nouvian-Dooghe Y. 1990. Immunolocalization of the cellular src protein in interphase and mitotic NIH c-src overexpresser cells. J Cell Biol 111:3097–3116.
Deacon NJ, Tsykin A, Solomon A, Smith K, Ludford-Menting M, Hooker DJ, McPhee DA, Greenway AL, Ellett A, Chatfield C, Lawson VA, Crowe S, Maerz A, Sonza S, Learmont , Sullivan JS, Cunningham A, Dwyer D, Mills J. 1995. Genomic structure of an attenuated quasi species of HIV-1 from a blood transfusion and recipients. Science 270:988–991.
Drakesmith H, Chen N, Ledermann H, Screaton G, Townsend A, Xu XN. 2005. HIV-1 Nef down-regulates the hemochromatosis protein HFE, manipulating cellular iron homeostasis. Proc Natl Acad Sci USA 102:11017–11022.
Fackler OT, Baur AS. 2002. Live and let die: Nef functions beyond HIV replication. Immunity 16:493–497.
Fackler OT, Wolf D, Weber HO, Laffert B, D'Aloja P, Schuler-Thurner B, Geffin R, Saksela K, Geyer M, Peterlin BM, Schuler G, Baur AS. 2001. A natural variability in the proline-rich motif of Nef modulates HIV-1 replication in primary T cells. Curr Biol 11:1294–1299.
Greenberg ME, Iafrate AJ, Skowronski J. 1998. The SH3 domain-binding surface and an acidic motif in HIV-1 nef regulate trafficking of class I MHC complexes. EMBO J 17:2777–2789.
Haller C, Rauch S, Fackler OT. 2007. HIV-1 Nef employs two distinct mechanisms to modulate Lck subcellular localization and TCR induced actin remodeling. PLoS ONE 2:e1212.
Hamilton JA. 2008. Colony-stimulating factors in inflammation and autoimmunity. Nat Rev Immunol 8:533–544.
Hanna Z, Kay DG, Rebai N, Guimond A, Jothy S, Jolicoeur P. 1998. Nef harbors a major determinant of pathogenicity for and AIDS-like disease induced by HIV-1 in transgenic mice. Cell 95:163–175.
Hanna Z, Weng X, Kay DG, Poudrier J, Lowell C, Jolicoeur P. 2001. The pathogenicity of human immunodeficiency virus (HIV) type 1 Nef in CD4C/HIV transgenic mice is fabolished by mutation of its SH3-binding domain, and disease development is delayed in the absence of Hck. J Virol 75:9378–9392.
Hashimoto S, Hirose M, Hashimoto A, Morishige M, Yamada A, Hosaka H, Akagi K, Ogawa E, Oneyama C, Agatsuma T, Okada M, Kobayashi H, Wada H, Nakano H, Ikegami T, Nakagawa A, Sabe H. 2006. Targeting AMAP1 and cortactin binding bearing an atypical src homology 3/proline interface for prevention of breast cancer invasion and metastasis. Proc Natl Acad Sci USA 103:7036–7041.
Hiyoshi M, Suzu S, Yoshidomi Y, Hassan R, Harada H, Sakashita N, Akari H, Motoyoshi K, Okada S. 2008. Interaction between Hck and HIV-1 Nef negatively regulates cell surface expression of M-CSF receptor. Blood 111:243–250.
Hung CH, Thomas L, Ruby CE, Atkins KM, Morris NP, Knight ZA, Scholz I, Barklis E, Weinberg AD, Shokat KM, Thomas G. 2007. HIV-1 Nef assembles a Src family kinase-ZAP-70/Syk-PI3K cascade to down-regulate cell surface MHC-I. Cell Host Microbe 1:121–133.
Kaplan KB, Swedlow JR, Varmus HE, Morgan DO. 1992. Association of $p60^{c\text{-}src}$ with endosomal membranes in mammalian fibroblasts. J Cell Biol 118:321–333.
Karkkainen S, Hiipakka M, Wang JH, Kleino I, Vaha-Jaakkola M, Renkema GH, Kiss M, Wagner R, Saksela K. 2006. Identification of preferred protein interactions by phage-display of the human Src homology-3 proteome. EMBO Rep 7:186–191.
Kasahara K, Nakayama Y, Ikeda K, Fukushima Y, Matsuda D, Horimoto S, Yamaguchi N. 2004. Trafficking of Lyn through the Golgi caveolin involves the charged residues on αE and αI helices in the kinase domain. J Cell Biol 165:641–652.
Kestler HW III, Ringler DJ, Mori K, Panicali DL, Sehgal PK, Daniel MD, Desrosiers RC. 1991. Importance of the nef gene for maintenance of high virus loads and for development of AIDS. Cell 65:651–662.
Kirchhoff F, Greenough TC, Brettler DB, Sullivan JL, Desrosiers RC. 1995. Brief report: Absence of intact nef sequences in a long-term survivor with nonprogressive HIV-1 infection. N Engl J Med 332:228–232.
Korade-Mirnics Z, Corey SJ. 2000. Src kinase-mediated signaling in leukocytes. J Leukocyte Biol 68:603–613.
Lerner EC, Smithgall TE. 2002. SH3-dependent stimulation of Src-family kinase autophosphorylation without tail release from the SH2 domain in vivo. Nat Struct Biol 9:365–369.
Ley SC, Marsh M, Bebbington CR, Proudfoot K, Jordan P. 1994. Distinct intracellular localization of Lck and Fyn protein tyrosine kinases in human T lymphocytes. J Cell Biol 125:639–649.
Lowell CA. 2004. Src-family kinases: Rheostats of immune cell signaling. Mol Immunol 41:631–643.
Mangasarian A, Piguet V, Wang JK, Chen YL, Trono D. 1999. Nef-induced CD4 and major histocompatibility complex class I (MHC-I) down-regulation are governed by distinct determinants: N-terminal alpha helix and proline repeat of Nef selectively regulate MHC-I trafficking. J Virol 73:1964–1973.
Matsuda D, Nakayama Y, Horimoto S, Kuga T, Ikeda K, Kasahara K, Yamaguchi N. 2006. Involvement of Golgi-associated Lyn tyrosine kinase in the translocation of annexin II to the endoplasmic reticulum under oxidative stress. Exp Cell Res 312:1205–1217.
Mitina O, Warmuth M, Krause G, Hallek M, Obermeier A. 2007. Src family tyrosine kinases phosphorylate Flt3 on juxtamembrane tyrosines and interfere with receptor maturation in a kinase-dependent manner. Ann Hematol 86:777–785.
Moarefi I, LaFevre-Bernt M, Sicheri F, Huse M, Lee CH, Kuriyan J, Miller WT. 1997. Activation of the Src-family tyrosine kianse Hck by SH3 domain displacement. Nature 385:650–653.
Oneyama C, Agatsuma T, Kanda Y, Nakano H, Sharma SV, Nakano S, Narazaki F, Tatsuta K. 2003. Synthetic inhibitors of proline-rich ligand-mediated protein-protein interaction: Potent analogs of UCS15A. Chem Biol 10:443–451.
Paliwal P, Radha V, Swarup G. 2007. Regulation of p73 by Hck through kinase-dependent and independent mechanisms. BMC Mol Biol 8:45.
Peterlin BM, Trono D. 2003. Hide, shield and strike back: How HIV-infected cells avoid immune eradication. Nat Rev Immunol 3:97–107.
Priceputu E, Hanna Z, Hu C, Simard MC, Vincent P, Wildum S, Schindler M, Kirchhoff F, Jolicoeur P. 2007. Primary human immunodeficiency virus type 1 Nef alleles show major differences in pathogenicity in transgenic mice. J Virol 81:4677–4693.
Pulvirenti T, Giannotta M, Capestrano M, Capitani M, Pisanu A, Polishchuk RS, San Pietro E, Beznoussenko GV, Mironov AA, Turacchio G, Hsu VW, Sallese M, Luini A. 2008. A traffic-activated Golgi-based signaling circuit coordinates the secretory pathway. Nat Cell Biol 10:912–922.
Roeth JF, Collins KL. 2006. Human immunodeficiency virus type 1 Nef: Adapting to intracellular trafficking pathways. Mol Biol Rev 70:548–563.
Saksela K, Cheng G, Baltimore D. 1995. Proline-rich (PxxP) motifs in HIV-1 Nef bind to SH3 domains of a subset of Src kinases and are required for the enhanced growth of Nef^{+} viruses but not for down-regulation of CD4. EMBO J 14:484–491.
Schwartz O, Marechal V, Le Gall S, Lemonnier F, Heard JM. 1996. Endocytosis of major histocompatibility complex class I molecules is induced by the HIV-1 Nef protein. Nat Med 2:338–342.
Suzu S, Tanaka-Douzono M, Nomaguchi K, Yamada M, Hayasawa K, Kimura F, Motoyoshi K. 2000. $p56^{dok\text{-}2}$ as a cytokine-inducible inhibitor of cell proliferation and signal transduction. EMBO J 19:5114–5122.
Suzu S, Harada H, Matsumoto T, Okada S. 2005. HIV-1 Nef interferes with M-CSF receptor signaling through Hck activation and inhibits M-CSF bioactivities. Blood 105:3230–3237.
Trible RP, Emert-Sedlak L, Smithgall TE. 2006. HIV-1 Nef selecyively activates Src family kinases Hck, Lyn, and c-Src through SH3 domain interaction. J Biol Chem 281:27029–27038.
Ueno T, Motozono C, Dohki S, Mwimanzi P, Rauch S, Fackler OT, Oka S, Takiguchi M. 2008. CTL-mediated selective pressure influences dynamic evolution and pathogenetic functions of HIV-1 Nef. J Immunol 180:1107–1116.
van't Hof W, Resh MD, 1997. Rapid plasma membrane anchoring of newly synthesized p59fyn: Selective requirement for NH_2-terminal myristoylation and palmitoylation at cysteine-3. J Cell Biol 136:1023–1035.

G Model
JVAC9554 1–7
ARTICLE IN PRESS

Vaccine xxx (2009) xxx–xxx

Contents lists available at ScienceDirect

Vaccine

journal homepage: www.elsevier.com/locate/vaccine

T cell-based functional cDNA library screening identified SEC14-like 1a carboxy-terminal domain as a negative regulator of human immunodeficiency virus replication

Emiko Urano[a,b], Reiko Ichikawa[a], Yuko Morikawa[b], Takeshi Yoshida[c], Yoshio Koyanagi[c], Jun Komano[a,*]

[a] National Institute of Infectious Diseases, 1-23-1 Toyama, Shinjuku-ku, Tokyo 162-8640, Japan
[b] Graduate School of Infection Control Sciences, Kitasato University, Shirokane 5-9-1, Minato-ku, Tokyo 108-8641, Japan
[c] Laboratory of Viral Pathogenesis, Institute for Virus Research, Kyoto University, Kyoto 606-8507, Japan

ARTICLE INFO

Article history:
Received 16 May 2009
Received in revised form 7 July 2009
Accepted 24 July 2009
Available online xxx

Keywords:
HIV-1
SEC14L1a
Genome-wide screening

ABSTRACT

Genome-wide screening of host factors that regulate HIV-1 replication has been attempted using numerous experimental approaches. However, there has been limited success using T cell-based cDNA library screening to identify genes that regulate HIV-1 replication. We have established a genetic screening strategy using the human T cell line MT-4 and a replication-competent HIV-1. With this system, we identified the C-terminal domain (CTD) of SEC14-like 1a (SEC14L1a) as a novel inhibitor of HIV-1 replication. Our T cell-based cDNA screening system provides an alternative tool for identifying novel regulators of HIV-1 replication.

1. Introduction

The molecular interaction between HIV-1 and the host is not fully understood. A systematic genome-wide approach provides the critical information for the completion of the HIV-1-host interactome. Many experimental genome-wide screening systems have been established to identify the cellular genes required for HIV-1 replication (Table 1, [1–8]). More than a hundred genes have been identified as being cellular factors that regulate HIV-1 replication. However, different screening systems do not identify the same set of genes, and many systems yielded non-overlapping candidates. These discrepancies are assumed to be due to differences in the experimental approaches, such as the virus, the cell line, or the genetic materials used.

For viruses, the wild-type HIV-1 [1,3–6] or a replication-incompetent HIV-1 pseudotyped with vesicular stomatitis virus (VSV)-G is used [2,7,8]. The VSV-G-pseudotyped "HIV-1-based vector" has been used to identify factors associated with the viral entry processes. However, in reality, it covers the events from post-membrane fusion to translation. One of the potential caveats in the use of the VSV-G-pseudotyped vector is that it enters cells via the VSV-G-restricted route, which is fundamentally different from the HIV-1 *Env*-mediated entry pathway [9–12]. The replication-competent HIV-1 should be ideal to cover the entire viral replication cycle; however, this may raise biosafety concerns.

For cells, non-T cells, such as a genetically engineered HeLa cells that ectopically express luciferase or beta-galactosidase (TZM-bl cells), are often used, since they are efficiently transduced with genetic materials [2,5–8]. Not many studies employ a T cell-based system, partly because genetic materials are not efficiently transduced into T cells [1,3,4]. To identify HIV-1 replication regulatory factors, it is preferable to perform the functional analysis in the natural targets of HIV-1 including T cells. The gene expression profile of non-T cells is apparently different from that of T cells as exemplified by the absence of T cell specific markers on non-T cells such as CD4. It is possible that a candidate gene isolated in the non-T cell-based system might not be expressed in T cells. It is impossible to identify T cell-specific factors in the non-T cell-based screening using the siRNA library or in the screening using cDNA libraries derived from non-T cells. Also, the effect or functions of some genes may not be identical in distinct cell types. The potential risk of a non-T cell-based assay is that we may falsely score a gene as a regulator of HIV-1 replication, although many genes have been discovered using non-T cell-based screening systems including the viral receptors. Ideally, the primary CD4-positive T cells, dendritic cells, macrophages, or NK/T cells should be used.

* Corresponding author at: AIDS Research Center, National Institute of Infectious Diseases, 1-23-1 Toyama, Shinjuku, Tokyo 162-8640, Japan. Tel.: +81 3 5285 1111; fax: +81 3 5285 5037.
E-mail address: ajkomano@nih.go.jp (J. Komano).

0264-410X/$ – see front matter © 2009 Published by Elsevier Ltd.
doi:10.1016/j.vaccine.2009.07.084

Table 1
Summary of genome-wide screening strategies to identify regulatory factors of HIV-1 replication.

Genetic material	Transduction approach	Cell line	Replication competency of HIV-1	Reference
cDNA library	Retroviral, stable	TE671	Incompetent	[2,8]
siRNA library	Transfection, transient	HeLa or 293T	Competent or incompetent	[5,6,7]
cDNA library	Lenti- or retroviral, stable	MT-4	Competent	[1,3,4]

Given technical limitations, this is currently unrealistic for genetic screening experiments.

As for the genetic material, cDNA libraries are often used [1–4,8]. Recent studies utilized siRNA libraries [5–7]. The cDNA approach is advantageous for providing genetic diversity. Expression of the full-length open reading frame of a gene can upregulate the function of the gene, whereas cDNA fragments can function in a diverse fashion. The gene silencing approach downregulates gene expression; however, the silencing efficiency of a gene varies in different cell types and at different time points in the assay (reviewed in [13]). As mentioned above, the gene silencing approach is unable to score the contribution of genes that are not expressed in the cells used in the assay.

The screening can be performed in cells that are either transiently [5–7] or stably [1–4,8] transduced with genetic materials. In the transient transfection assays, it is possible that the dysregulation of a gene function can damage the physiology of the cells. In such a case, the inhibition of HIV-1 replication can be observed, but may not be a direct inhibitory effect of the gene of interest. Such a risk can be minimized by using cells stably transduced with the genetic materials.

We conducted a phenotype cDNA screen using a T cell line-based assay to identify cellular genes that render cells resistant to HIV-1 replication [3]. The advantage of our functional screening system is that cDNA libraries are stably transduced into cells, and that a replication-competent HIV-1 and a human T cell line MT-4 are used. With this system, we have successfully identified the SEC14-like 1a (SEC14L1a) C-terminal domain (CTD) as an inhibitor of HIV-1 replication that targets the late phase of the viral life cycle.

2. Materials and methods

2.1. Cells, transfection, cDNA selection

Cells were maintained in RPMI 1640 medium (Sigma, St. Louis, MA) supplemented with 10% fetal bovine serum (Japan Bioserum, Tokyo, Japan), 100 U/ml penicillin, and 100 μg/ml streptomycin (Invitrogen, Tokyo, Japan). Cells were incubated at 37 °C in a humidified 5% CO_2 atmosphere. Cells were transfected with Lipofectamine 2000 according to the manufacturer's protocol (Invitrogen). The method of selecting human cDNAs that confer resistance to HIV-1 has been described previously in detail [3].

2.2. Plasmids

The SEC14L1a CTD1 was amplified from MT-4 polyA RNA by reverse transcriptase PCR (RT-PCR) using the primers 5'-GCACCGGTCTCGAGCCACCATGGACTACAAAGACGATGACGACCCTGCGTGCGCCGCCAGCAGC-3′ and 5'-CCAATTGCTACCTGGAGATCATGGAGCTG-3'. The SEC14L1a CTD2 was amplified by PCR from human lymph node cDNA library (Takara, Otsu, Japan) using the primers 5'-GCACCGGTCTCGAGCCACCATGGACTACAAAGACGATGACGACTGCGAAGTGCCAGAGGGTGGAC-3' and 5'-CCAATTGCTACCTGGAGATCATGGAGCTG-3'. Full length (FL) SEC14L1a was amplified by PCR from a plasmid containing the SEC14L1a open reading frame (ORF, CS0DL004YN18, Invitrogen), using the primers 5'-GCACCGGTCTCGAGCCACCATGGACTACAAAGACGATGACGACGTGCAGAAATACCAGTCCCCAG-3' and 5'-CCAATTGCTACCTGGAGATCATGGAGCTG-3'. The AgeI-MfeI fragments of the PCR products were cloned into the XmaI-MfeI sites of the pEGFP-C3 plasmid (Clontech, Palo Alto, CA), generating pEGFP-SEC14L1a-CTD1, -CTD2, and -FL. The XhoI-MfeI fragments from the resulting plasmids were cloned into the corresponding restriction sites of the pCMMP KRAB vector, creating pCMMP GFP-SEC14L1a-CTD1, -CTD2, and -FL. The HIV-1 *tat* was amplified by PCR using the primers 5′-AACCGGTCTCGAGCCACCATGGAGCCAGTAGATCCTAGAC-3′ and 5′-GGATCCTCAGTCGTCATCGTCTTTGTAGTCTTCCTTCGGGCCTGTCGGGTC-3′. A Tat expression vector pCMMP Tat was constructed by cloning the AgeI-BamHI fragment of the PCR product into the corresponding restriction sites of the pCMMP KRAB vector. The HIV-1 *Env* and GFP expression vectors (pIIIex and pCMMP GFP, respectively) are described previously [3,12,14]. To construct the pCMMP GFP-FLAG (GFPf), pCMMP CXCR4 d-10 [15] was digested with AgeI and XhoI to remove CXCR4 d-10 ORF and self-ligated after blunting with T4 DNA polymerase. The HIV-1 *gag-pol*, *tat*, and *rev* expressing plasmid pCMVR8.91 was a generous gift from Dr. Trono's group [16].

2.3. Western blotting

Western blotting was performed according to techniques described previously [17]. The following reagents were used: anti-FLAG (rabbit polyconal, 600-401-383, Rockland, Gilbertsville, PA), anti-p24 (183-H12-5C, NIH AIDS Research and Reference Reagent Program), anti-gp120 (vA-20 and vT-21 antibodies, Santa Cruz Biotech, Santa Cruz, CA), biotinylated anti-goat antibody (GE Healthcare Bio-Sciences, Piscataway, NJ), horseradish peroxidase-conjugated streptoavidin (GE Healthcare Bio-Sciences), and EnVision+ system (Dako, Glostrup, Denmark). Signals were visualized with an LAS3000 imager (Fujifilm, Tokyo, Japan) and quantified by Multi Gauge ver 3.0 software (Fujifilm).

2.4. Confocal microscopy

293T cells transiently transfected with expression vectors for SEC14L1a derivatives were grown on glass plates, fixed in 4% formaldehyde in phosphate buffer saline (PBS) for 5 min at 24 h post-transfection, stained with Hoechst 33258 (Sigma), mounted (Vectorshield, Vector Laboratories, Burlingame, CA), and imaged using a confocal microscope META 510 (Carl Zeiss, Tokyo, Japan). For MT-4 cells, live cells were incubated with Hoechst 33258 and imaged unfixed. Image brightness and contrast were processed by META510 software (Carl Zeiss).

2.5. Immunoprecipitation

Cells expressing FLAG-tagged proteins were harvested and washed twice with PBS and then lysed in the lysis buffer (50 mM Tris–HCl, pH 8.0, 0.5% IGEPAL CA630, protease inhibitor cocktail from Sigma) on ice for 30 min. The soluble fraction was obtained by centrifugation at 15,000 rpm for 30 min at 4 °C, and was incubated with 20 μl of Red-Anti-FLAG M2 Affinity Gel (Sigma) with gentle mixing overnight at 4 °C. After washing the agarose beads for five times with the lysis buffer, the bound complexes were eluted with the FLAG peptide, and analyzed by Western blotting.

Please cite this article in press as: Urano E, et al. T cell-based functional cDNA library screening identified SEC14-like 1a carboxy-terminal domain as a negative regulator of human immunodeficiency virus replication. Vaccine (2009), doi:10.1016/j.vaccine.2009.07.084

2.6. Flow cytometry

Cells were labeled with PE-Cy5-conjugated anti-CD4 antibody or PE-conjugated anti-CXCR4 antibody (Beckton Dickinson, San Jose, Calif.) for 30 min at 4 °C. Cells were washed once with PBS supplemented with 1% FBS and analyzed by FACS Aria (Beckton Dickinson). The GFP-positive cells were sorted using FACS Aria.

2.7. Monitoring HIV-1 replication

For HIV-1 infection, 1×10^5 cells were incubated at the room temperature with the HIV-1_{HXB2}-containing culture supernatant, which had approximately 1.0 ng of $p24^{CA}$, for approximately 30 min. The culture supernatants were collected at 4 d post-infection and subjected to ELISA to measure the $p24^{CA}$ antigen, using a Retro TEK p24 Antigen ELISA Kit according to the manufacturer's protocol (Zepto Metrix, Buffalo, NY). The signals were measured with an ELx808 microplate photometer (BIO-TEK®, Winooski, VT).

2.8. PCR analysis

The cellular DNA and RNA were extracted from cells infected with VSV-G-pseudotyped HIV-1 vector produced by using pNL-Luc plasmid, as described previously [17]. The Alu-LTR PCR and RT-PCR were performed as described previously [3,17] using the following primers: for the first Alu-LTR PCR reaction, 5'-AACTAGGGAACCCACTGCTTAAG-3' and 5'-TGCTGGGATTACAGGCGTGAG-3'; and for the second Alu-LTR PCR reaction, 5'-AACTAGGGAACCCACTGCTTAAG-3' and 5'-CTGCTAGAGATTTTCCACACTGAC-3'. For amplification of HIV-1 mRNA, 5′-ATGGAGCCAGTAGATCCTAGAC-3′ and 5′-CTATTCCTTCGGGCCTGTCGGG-3′ primers were used. For the control, we amplified beta-globin and cyclophilin A using the following primers: beta-globin, 5'-TATTGGTCTCCTTAAACCTGTCTTG-3' and 5'-CTGACACAACTGTGTTCACTAGC-3'; and cyclophilin A, 5′- CACCGCCACCATGGTCAACCCCACCGTGTTCTTCGAC-3′ and 5′- CCCGGGCCTCGAGCTTTCGAGTTGTCCACAGTCAGCAATGG-3′. The amplicons were separated in a 2% agarose gel, stained with ethidium bromide, and imaged with a Typhoon scanner (GE Healthcare Bio-Sciences).

2.9. Collection of virus-like particle

Tissue culture supernatants containing virus-like particles (VLP) were passed through nitrocellulose filters (0.45 μm, Millipore, Tokyo, Japan) and the virions were collected by centrifugation (Optima™ TL, TLA 100.3 rotor, 541 k × *g* for 1 h; Beckman Coulter, Miami, FL).

3. Results

3.1. Identification of SEC14L1a as a potential regulator of HIV-1 replication

We prepared MT-4 cells that constitutively express cDNA transduced by a lentiviral vector or an MLV-based retroviral vector (Fig. 1A). The cDNAs were derived from human peripheral blood mononuclear cells (PBL) and *Oryctolagus cuniculus* (European rabbit) kidney-derived cell line RK13 cells. MT-4 cells transduced with cDNA were collected by FACS sorter using the green fluorescence as a marker since viral vectors encoded the GFP expression cassette. Then, cells were infected with HIV-1. Surviving cells were propagated and the genomic DNA was extracted to recover the transduced cDNA by PCR as previously described [3]. We isolated two clones encoding the carboxy terminal domain (CTD) of SEC14L1a (Gene ID 6397, Fig. 1B and C); one from the PBL cDNA library (1/65 independent clones, 1.5%), and one from the RK13 cDNA library (1/42 independent clones, 2.4%). The fact that the SEC14L1a CTD was successfully identified from two independent cDNA libraries strongly suggests that it is a negative regulator of HIV-1 replication. It is important to note that previous genome-wide screenings for HIV-1 regulators have not identified SEC14L1a CTD. This clearly suggests that our T cell-based cDNA screening system is unique, and should be able to complement the other genome-wide screening systems.

SEC14L1a belongs to the widely-expressed SEC14-superfamily that is involved in membrane trafficking and phospholipid metabolism [18–21]. The function of SEC14L1a is not well understood. The C-terminus of SEC14L1a encodes a Golgi dynamics (GOLD) domain (amino acids (aa) 523–674; Fig. 1C) that mediates the protein-protein interaction possibly involved in the maintenance of Golgi apparatus function and vesicular trafficking [22]. The only reported biological activity of SEC14L1a is to interact with cholinergic receptors AchT and CHT1 [23]. The GOLD domain is responsible for the physical interaction between SEC14L1a and cholinergic receptors. However, the functional significance of these interactions remains to be clarified. The conserved SEC14 domain directly interacts with lipid molecules [17–21]. However, the lipid ligand of SEC14L1a (aa 319–490, Fig. 1C) has yet to be identified.

3.2. Construction of expression vectors for SEC14L1a derivatives

The longest SEC14L1a cDNA recovered from the PBL cDNA library spanned nucleotides (nt) 2045–2492 of SEC14L1a mRNA (NM_003003.3), covering the CTD of the SEC14L1a open reading frame (ORF; Fig. 1B). We detected a potential translational start codon at nt 2188-2190 within the GOLD domain (asterisk, Fig. 1B). We speculated that the isolated cDNA might have expressed the carboxy half of the GOLD domain (aa 641–715) in MT-4 cells, leading to the inhibition of HIV-1 replication.

To test this, we constructed an expression plasmid for FLAG-tagged CTD (aa 642-715) fused to the carboxy terminus of GFP (CTD1; Fig. 1C). We also constructed GFP fusion proteins spanning the GOLD domain (CTD2, aa 493–715) or the full-length SEC14L1a (FL; Fig. 1C). Expression of these proteins was verified by Western blotting of transient transfected 293T cells (Fig. 1D). The confocal microscopy analysis indicated that the FL localized mainly in the cytoplasm, with some accumulation in the perinuclear regions (Fig. 1E), consistent with a previous report [23]. CTD1 was distributed in the cytoplasm and the nucleus, with a slight preference for the cytoplasm. CTD2 was evenly distributed to the nucleus and cytoplasm. When MT-4 cells constitutively expressing FL, CTD1, and CTD2 were analyzed, the subcellular distribution was less clear, due to the small cytoplasm (Fig. 1F). However, FL was distributed evenly to the nucleus and cytoplasm in MT-4 cells. In contrast, CTD1 was excluded from the nucleus in MT-4 cells (Fig. 1F). The distribution of CTD2 in MT-4 cells was similar to that in 293T cells (Fig. 1F). The differences of protein distribution in two cell types may be caused by the cell type-dependent regulation of protein trafficking and/or the effect of protein expression levels.

3.3. Verification of anti-HIV-1 activity associated with SEC14L1a CTD1

We introduced FL, CTD1, or CTD2 into MT-4 cells using the MLV vector, and isolated cells constitutively expressing FL, CTD1, or CTD2. Expression of SEC14L1a derivatives in MT-4 cells was verified by Western blotting (Fig. 2A). FL expression was verified by immuno-precipitation assay (Fig. 2A). The detection of FL by Western blotting was inefficient considering the fact that all the SEC14L1a derivatives are GFP-tagged, and the GFP intensity of FL-expressing MT-4 cells was not lower than that of CTD1-expressing

Please cite this article in press as: Urano E, et al. T cell-based functional cDNA library screening identified SEC14-like 1a carboxy-terminal domain as a negative regulator of human immunodeficiency virus replication. Vaccine (2009), doi:10.1016/j.vaccine.2009.07.084

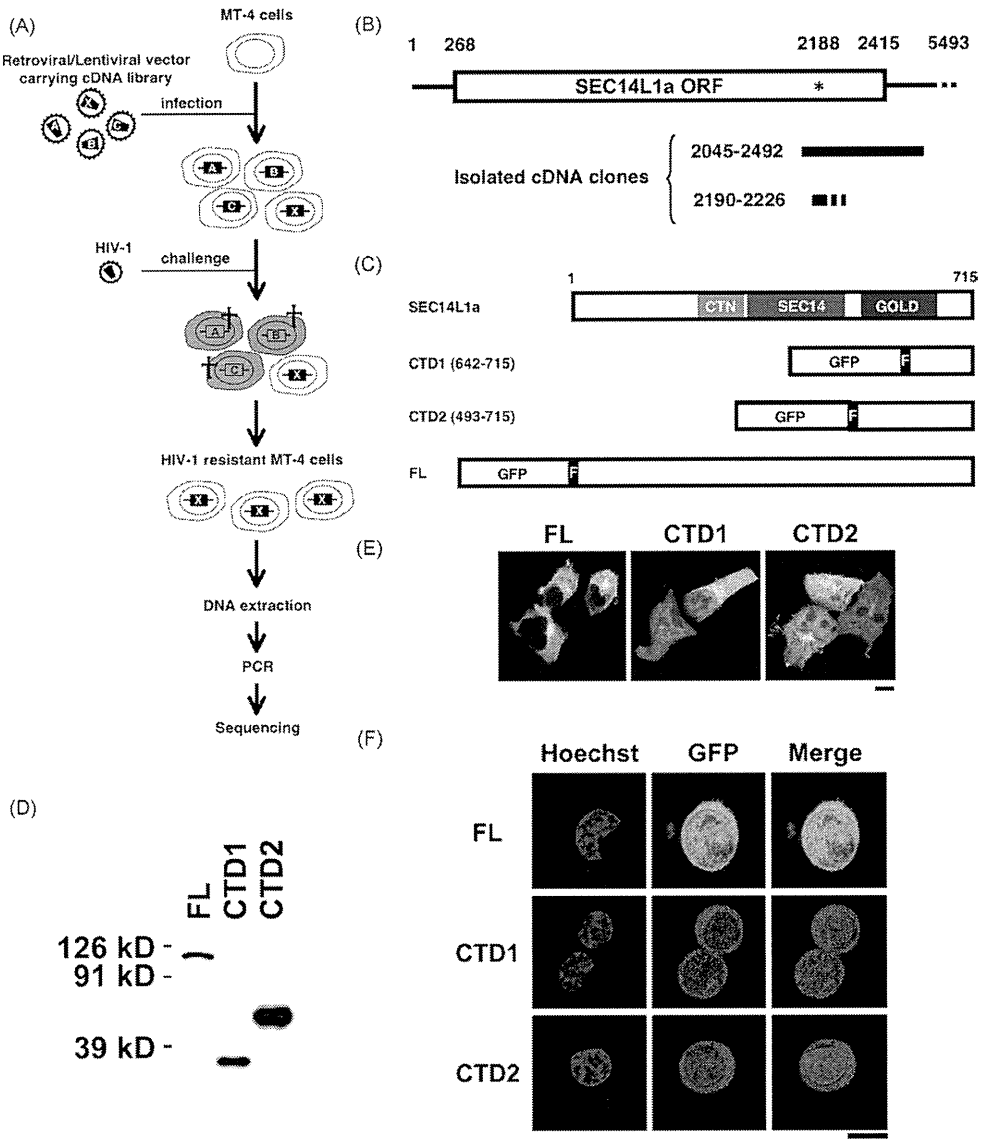

Fig. 1. Identification of SEC14L1a CTD as a potential regulator of HIV-1 replication. (A) The experimental strategy used to screen a cDNA library for genes rendering cells resistant to HIV-1. MT-4 cells were infected with a retroviral or lentiviral vector carrying cDNA libraries and were challenged with wild-type HIV-1_{HXB2}. The HIV-1-infected cells (gray with cross) quickly undergo cell death. The surviving cells were propagated, collected, and the transduced cDNA labeled X was determined. (B) Schematic representation of SEC14L1a mRNA (NM_00303.3) and the isolated gene fragments. The open reading frame (ORF) is assigned from nucleotides (nt) 268 to 2415. The potential internal translational initiation codon is marked with an asterisk. (C) Schematic representation of the SEC14L1a protein (NP_002994). SEC14L1a has a CRAL_TRIO_N domain (CTN, amino acids 241–313), a SEC14p-like lipid-binding domain (SEC14, amino acids 319–490), and a Golgi dynamics domain (GOLD, amino acids 523–674). The cloned fragments (CTD1 and CTD2) and full-length (FL) gene were tagged with a FLAG epitope (indicated with an "F") on their N-termini, and fused to the C-terminus of GFP. (D) Verification of FL, CTD1, and CTD2 expression in 293T cells by Western blotting using anti-FLAG antibody. (E) Confocal microscopy images of 293T cells expressing FL, CTD1, or CTD2. The green signal represents GFP fluorescence. Magnification, 630×; scale bar, 10 μm. (F) Confocal microscopy images of MT-4 cells constitutively expressing FL, CTD1, or CTD2. The blue signal represents the Hoechst-stained nucleus, and green represents GFP fluorescence. Magnification, 630×; scale bar, 5 μm.

cells (Fig. 1F). The MLV vector expressing GFP alone was used as a control. The cell proliferation, morphology, and cell surface levels of HIV-1 receptors were unaltered by any of the SEC14L1a derivatives (Fig. 1F, 2B, and data not shown). HIV-1 replication was tested in these cells. The level of HIV-1 replication was significantly inhibited in CTD1- and CTD2-expressing cells (69.1% and 69.8% on the average from seven independent experiments, respectively, $P < 0.05$, two-tailed Student's t-test), but was hardly inhibited in FL-expressing cells (86.4%, not statistically significant; Fig. 2C). This observation was reproducible in independently established MT-4 cells and SupT1 cells (data not shown). These data verified the original screening results, and suggest that the C-terminal half of GOLD domain of SEC14L1a serves as an inhibitor of HIV-1 replication. In contrast, it is suggested that FL is not a potent negative regulator of HIV-1 replication.

3.4. SEC14L1a CTD1 and CTD2 target the late phase of the HIV-1 life cycle

We analyzed the viral entry and production phases to determine which step of the HIV-1 life cycle CTD1 and CTD2 target.

The Alu-LTR PCR assay was performed to examine the effect of SEC14L1a derivatives on the viral entry phase. The MT-4 cells stably expressing GFP, FL, CTD1, or CTD2 were infected with VSV-

Please cite this article in press as: Urano E, et al. T cell-based functional cDNA library screening identified SEC14-like 1a carboxy-terminal domain as a negative regulator of human immunodeficiency virus replication. Vaccine (2009), doi:10.1016/j.vaccine.2009.07.084